Master Thesis

INTERCOMPARISON OF TOP OF ATMOSPHERE REFLECTANCES MEASURED BY GOME AND ATSR-2 ON BOARD ERS-2

Author:

Chinonso C. Unaichi

Reviewers:

Prof. John. P. Burrows

Dr. Mark Weber

Supervisor:

Dr. Mark Weber

Institute of Environmental Physics and Remote Sensing (IUP-IFE)

University of Bremen, Bremen, Germany

January 5, 2016

I hereby declare that all the contents of this work is written on my own and only with the means as indicated. I also give permission for the digital version of my thesis to be made available on the webpage at Postgraduate Program ENVIRONMENTAL PHYSICS (PEP) research archive.

Chinonso C. Unaichi

Contents

Abstract

The Global Ozone Monitoring Experiment (GOME) and Along Track Scanning Radiometer - Two (ATSR-2) on board European Remote Sensing Satellite - Two (ERS-2) measure reflectance at the top of earth's atmosphere. GOME measures top of atmosphere reflectance in the UV-VIS (240 - 790nm) wavelength region by scanning across track (East, West, Nadir, and Fly-back) leading to four GOME ground pixels. ATSR-2 is a highly calibrated instrument that measures reflectance in the VIS - Infrared region, it scans along track with dual view geometry (Nadir and Forward scan). GOME channels 3 and 4 overlap with the ATSR-2 channels centered at 555nm and 659nm are used for the reflectance intercomparison study. Data from July 1997 to June 2002: GOME level 1B Nadir reflectance spectra (V5) and ATSR-2 gridded reflectance data available from July 1997 to July 2002, resampled to 1km $\times$ 1km along track are used.

Spectrally averaged GOME and spatially averaged ATSR-2 reflectances are derived and separated into different scenarios (All scene, cloudy, dark, and bright scenes). Thus, it is demonstrated in this work that the GOME-1 version 5 data without the correction factor have a strong linear relation with the highly calibrated ATSR-2 measurements at 555nm and 659nm for all scenarios (for January and July 1997 - 2002 data). On average GOME overestimate top of the atmosphere reflectance by $\sim 11\%$ as compared to ATSR-2.

Chapter 1

Introduction

1.1 Motivation

In order to obtain useful information about earth's surface or atmosphere, remote sensing techniques are employed to measure the reflected or emitted electromagnetic radiation at the top of the atmosphere. The amount of energy or radiation measured is dependent on the properties (chemical, physical, and structural) of the surface, angle of incidence, wavelength, and intensity of the incident electromagnetic radiation. Measurement of the top of atmosphere reflectance is important in the global retrieval of earth's atmospheric species and surface properties, as the measured reflectance carries information about different atmospheric species, clouds, aerosols, and surface properties.

Over the years a number of satellite instruments with different measurement techniques have been launched to measure the earth's radiance and solar irradiance at the top of the atmosphere. To obtaining accurate information of the measured variables (earth's radiance and solar irradiance), the radiometric calibration of the satellite instrument is paramount [Koelemeijer et al.,1998]. In this work reflectance validations is carried out by doing an intercomparison of the top of atmosphere reflectance measured by GOME [Burrows et al.,1999] and ATSR-2 [North et al.,1999] instruments on board of ERS-2. Since both instruments are on board the same satellite, the illumination geometry is nearly identical, and their measurements can be collocated accurately in space and time allowing the investigation of radiometric calibration of GOME by comparison to ATSR-2. Also ATSR-2 is a low noise detector with high quality calibration and stable over a long period of time. ATSR-2 has a designed accuracy of 2% [Mutlow et al.,1999] for the reflectivity measurements, and GOME radiance and irradiance measurements with a designed accuracy of 3 - 3.5%[Bednarz 1995].

There are several studies that have been carried out intercomparing measurements from GOME and ATSR-2 on board ERS-2. [Koelemeijer et al.,1998] carried out comparison study of visible calibration of GOME and ATSR-2 on board ERS-2, by investigating the reflectivity of the earth (centered at 555 nm and 659 nm) measured by both instruments. The data analyzed is from collocated partly cloudy scenes over the Atlantic ocean acquired on 23 July 1995. From the result, reflectivity measured by both instruments agree well. The reflectivity of ATSR-2 was observed to be systematically lower than that of GOME by 4.0% and 2.2% (relative differences) for measurements around 555nm and 659nm respectively. Also [Rozanov et al.,2006] carried out an intercomparison of cloud top heights derived using GOME and ATSR-2 instruments.

In this study, global visible reflectance validation has been carried out using radiation measured by GOME and ATSR-2 from July 1996 to July 2003. The aim is to carefully characterize the reflectances spectrally, spatially and also temporally to allow for trends investigation. The validation strategy used in this study has been adopted from the SCILOV (SCIAMACHY long term validation) project, from the intercomparison of TOA reflectances measured by SCIAMACHY and MERIS on board ENVISAT. The ground pixels were separated into different scenarios (cloudy and cloud free pixels) using cloud parameter (Cloud fraction) and spectral surface reflectivity. The advantage of carrying out the comparison in this manner is the improved comparability with SCILOV results.

1.2 Cloud fraction

Clouds have a strong impact on water cycle and earth's radiation budget, therefore an accurate knowledge of cloud coverage or parameter is important to understanding global climate. Cloud properties information originate from the interaction of solar or terrestrial radiation with cloud. Cloud fraction is described as the fraction of super-pixel with cloud [Sayer et al.,2010]. It ranges from 0 to 1, i.e for CF = 0, which implies completely cloud free pixels and CF = 1, implies completely cloudy pixels. Accurate knowledge of cloud fraction is essential for the evaluation of global climate models. It is also important to derive cloud fraction from radiation measurement retrieved by high spatial resolution instrument. By offering good spatial coverage, visible and infrared imaging instruments have been used to derive long time series of cloud properties. In this study GRAPE [Sayer et al.,2011] cloud fraction data derived from the highly calibrated ATSR-2 instrument have been used. Figure 1.1 shows the GRAPE

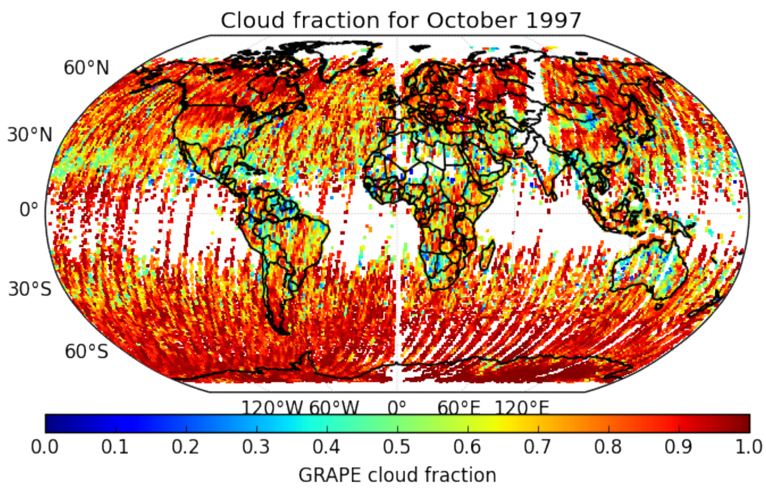

Figure 1.1: Global cloud fraction for October 1997

cloud fraction derived from ATSR-2 measurement for the October 1997. The GRAPE dataset is internally flagged as *high quality*: where there is a good consistency between the measurements and the retrieved state, and *bad quality* data [Sayer et al.,2011]. Since

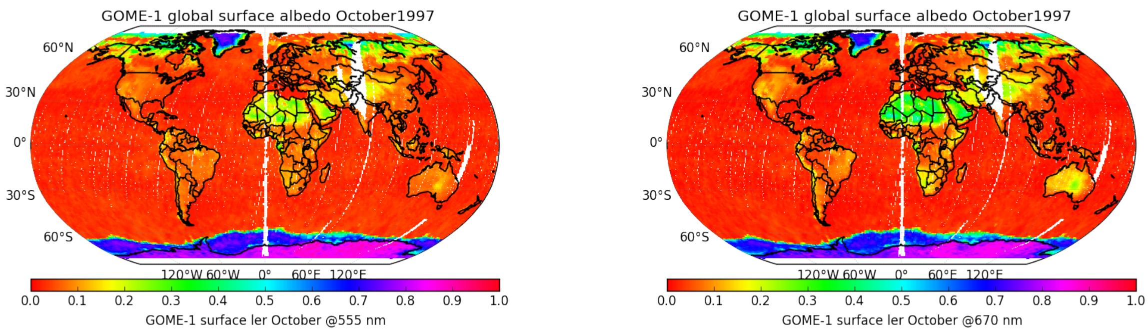

Figure 1.2: Global surface spectral albedo derived from GOME-1 TEMIS ler climatology data at 555nm and 670 nm for October 1997.

its recommended to consider only the high quality data, only high quality cloud fraction data are read out, resulting to missing pixels as seen in Figure 1.1.

1.3 Spectral surface albedo

The albedo of a surface is the amount of incident radiation that is been reflected back to the space. Under cloud free condition, larger component of the reflected radiation is as a result of surface reflection. Therefore the knowledge of spectral surface albedo is important for trace gases retrievals and also to derive aerosol and cloud properties. Earth consist of different surface types (Oceans, sea ice, snows, Lakes, Deserts, Forests), all having different surface reflectivity. Oceans, forests and lakes have relatively small surface reflectivity. Table 1.1 below shows estimates of albedo for different surfaces.

The TEMIS lER climatology database [Koelemeijer et al.,2003] at 555 nm and 670 nm have been used in this study to subdivide the GOME cloudy free pixels (GOME pixels with CF < 0.2) into dark and bright scenes.

Table 1.1: Table of estimated surface albedo for different surface, data from [Coakley, J. A.,2003].

Surface type	Albedo
Forests (tropical broadleaved forest)	0.12 - 0.15
Ocean	0.07
Desert	0.36
Snow	0.66
Sea ice	0.62

1.4 Outline of the thesis

The thesis starts in Chapter 2 with a brief theoretical background on electromagnetic radiation and their interaction with the earth surface. It includes a short description of electromagnetic wave, polarization of electromagnetic wave, angular distribution of radiation at the top of the atmosphere and electromagnetic spectrum. In Chapter 3 the satellite instruments of interest are described. It includes a short history on the European Remote Sensing Satellite Two (ERS-2), description of the viewing geometries of GOME ATSR-2 instruments and also their radiometric properties . Chapter 4 starts with a short description of data used in this study and follows with step by step description of the intercomparison method. In Chapter 5 results and analysis of are discussed and In Chapter 6 the conclusion, a brief summary of the work and outlook are presented. Further plots are shown in the appendix.

Chapter 2

Theoretical Background

2.1 Electromagnetic radiation

Electromagnetic radiation is a prerequisite for earth observation, as it contains useful information about the surface materials and atmosphere after it interacts with the earth's atmosphere or it's emission from the earth's surface. Electromagnetic radiation propagates as a wave motion with the speed of light (c = 3×10^8 m/s). The radiation consist of electric ($\vec{E}$) and magnetic ($\vec{B}$) field perpendicular to the direction of the propagation. Therefore, the propagating plane wave with:

$$\vec{E} = \begin{pmatrix} E_x \\ E_y \\ E_z \end{pmatrix} = \begin{pmatrix} E_0 \cos(\omega t - kz) \\ 0 \\ 0 \end{pmatrix}$$

$$\vec{B} = \begin{pmatrix} B_x \\ B_y \\ B_z \end{pmatrix} = \begin{pmatrix} 0 \\ \frac{E_0}{c^2} \cos(\omega t - kz) \\ 0 \end{pmatrix}$$

satisfy the Maxwell's equations for free space

$$\vec{\nabla} \cdot \vec{E} = 0 \tag{2.1}$$

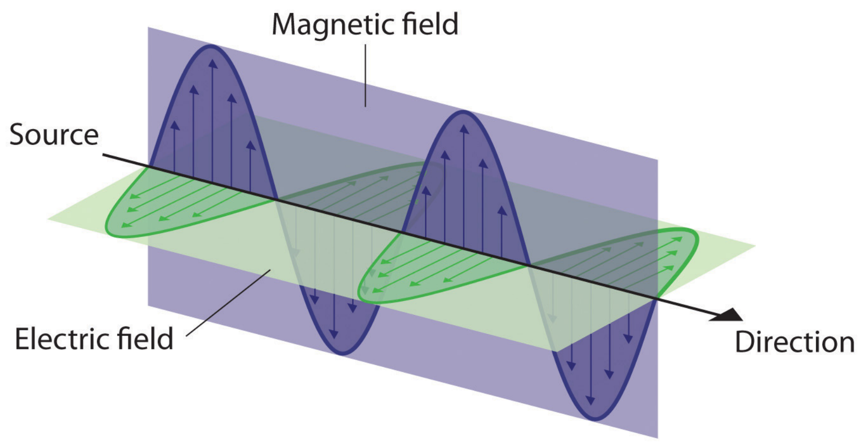

Figure 2.1: Electromagnetic wave [credit:2012books.lardbucket.org]

$$\vec{\nabla} \cdot \vec{B} = 0 \tag{2.2}$$

$$\vec{\nabla} \times \vec{E} = -\frac{\partial \vec{B}}{\partial t} \tag{2.3}$$

$$\vec{\nabla} \times \vec{B} = \varepsilon_0 \mu_0 \frac{\partial \vec{E}}{\partial t} \tag{2.4}$$

here, $\vec{E}$ and $\vec{B}$ are the electric and magnetic field vectors of the wave, ε_0 and μ_0 are the electric permittivity and the magnetic permittivity of the free space. The velocity of the electromagnetic radiation in space is:

$$c = \frac{\omega}{k} = \frac{1}{\sqrt{\varepsilon_0 \mu_0}} \tag{2.5}$$

where c is the speed of light, ω is the angular frequency and k is the wave number. The angular frequency and wave number are used to characterize electromagnetic wave and are related to frequency f and wavelength λ, and respectively as follow:

$$\omega = 2\pi f \tag{2.6}$$

$$k = \frac{2\pi}{\lambda} \tag{2.7}$$

2.2 Polarization

polarization is one of the physical properties of electromagnetic wave, it tells how the direction of the electric and magnetic field vectors varies with time. The electromagnetic wave is *linearly* polarized, if the electric field is parallel to the x-axis and the magnetic field parallel to the y-axis. Thus *circularly* polarized, if the field vectors rotate in xy-plane with a fixed amplitude. The combination of linearly and circularly polarized light is called elliptically polarized light. Also light is *randomly* polarized (unpolarized) if the direction of the field vectors change randomly on a short time scale. Radiation from the sun is randomly polarized or unpolarized, in nature polarization is caused when solar radiation is scattered by atmospheric components (aerosols, cloud particles, air molecules) and earth surface (vegetation, ice, soil, ocean,). However there are various approaches to correct for the polarization effect in the retrieved data product.

In remote sensing, polarization effect may affect accurate measurements of satellite instruments. Instruments that are sensitive to the polarization state of the observed radiation tend to generate biased measurement [Boettger et al.,2006]. GOME is a polarization sensitive instrument, in it polarization measuring device (PMD) is installed to correct for the polarization effect.

2.3 Top of the atmosphere reflectance

Electromagnetic radiation from the Sun traveling through the atmosphere can interact with atmospheric molecules and particles by reflection, scattering, and absorption. These mechanisms are directly proportional to

- the intensity of the radiation at that point along the light path
- the nature of the scattering or absorbing medium
- the concentration of the absorbing or scattering molecules and particles

Thus on interaction, the radiation encounters a number of changes in path, wavelength, magnitude, phase and polarization. Scattering and reflection of light from the earth's surface and atmosphere are useful for several retrieval techniques in remote sensing application. Top of the atmosphere reflectance observed by satellite instruments, is used to retrieve atmospherics parameters like, aerosol (optical depth and type), cloud parameters (optical thickness and height), vertical profiles of trace gases, solar UV irradiance variability and more [Burrows et al.,1999].

2.3.1 Distribution of radiation

In remote sensing, it is important to understand the angular distribution of radiation in space. Therefore analysis of radiation field in space demands the consideration of the amount of radiant energy with a certain solid angle Ω. The solid angle is the ratio of the area a, of a spherical surface intercepted at the core to the square of the radius R.

$$\Omega = \frac{a}{R^2} \ (sr) \tag{2.8}$$

for differential area in polar coordinates

$$d\Omega = \sin\vartheta d\vartheta d\varphi \tag{2.9}$$

here ϑ is the zenith angle and φ is the azimuth angle.

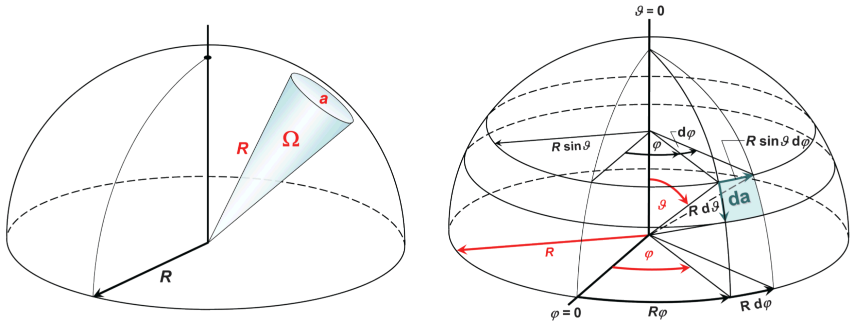

Figure 2.2: Solid angle within a sphere [seos-project.eu,2015].

The power Φ incident on an element dA is proportional to dA and $d\Omega$ also with the intensity of the radiation I given by

$$d\Phi = I\cos\vartheta dA d\Omega \tag{2.10}$$

where $\cos\vartheta$ dA is the effective area at which the radiation is being intercepted. From Equation 2.10 we can therefore define the radiance (or intensity) as the integral, of the power incident in a specific direction traveling through a unit area per unit time at a specific wavelength range over some finite range of electromagnetic spectrum.

$$I = \frac{d\Phi}{\cos\vartheta dA d\Omega} \ (Wm^{-2}nm^{-1}sr^{-1}) \tag{2.11}$$

The total incident power per unit area is called the irradiance *E*. It is obtained by integrating equation (2.11) over the entire hemisphere of solid angles lying above the plane.

$$E = \int_0^{\frac{\pi}{2}} \int_0^{2\pi} I \cos\vartheta d\Omega \;\; (Wm^{-2}nm^{-1}) \tag{2.12}$$

2.4 Electromagnetic spectrum

Electromagnetic radiation is composed of bands or groups of waves propagating through a vacuum. These waves show a continuous range of wavelengths, the whole range or the integrality of these waves is called electromagnetic spectrum. Thus, radiation can be associated with a particular part of the spectrum by noting the effects it produces when it interacts with a certain material [Wallace and Hobbs 2006]. The difference between the different regions of the electromagnetic spectrum is the amount of energy found in their photons, given by

$$E_p = \frac{hc}{\lambda} \tag{2.13}$$

here h is the Plank constant (6.62×10^{-34} J.sec).

Different terms are used to describe different parts of the spectrum as shown in Figure 2.3, which shows the names and portion of the electromagnetic spectrum of interest in remote sensing. The UV, VIS and Infrared regions play a vital role in the earth's energy balance and atmospheric remote sensing.

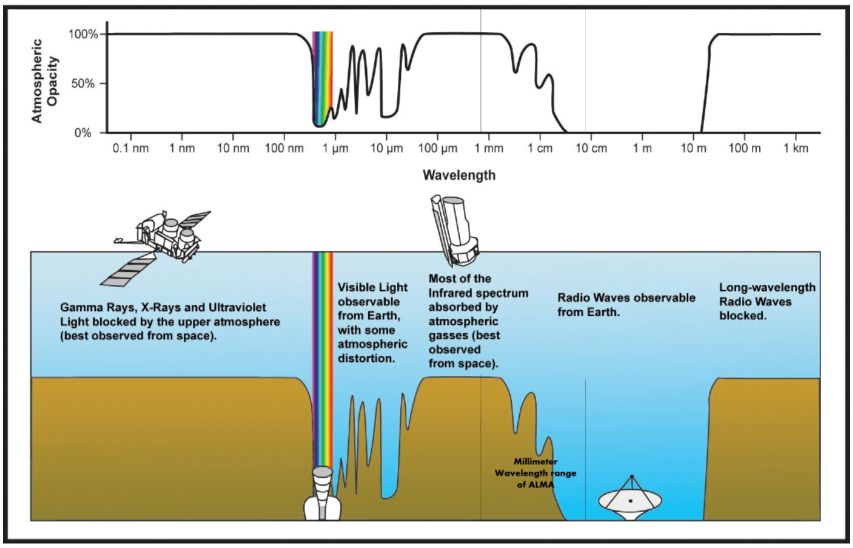

Figure 2.3: Electromagnetic spectrum [Credit: Wikimedia, T.Reyes]

2.4.1 Solar spectrum

The sun which is the source of solar radiation, with a surface temperature of 5800 K, spaced from the Earth at a distance of $\approx 150\times10^6$ km. Thus, due to the elliptical orbit of the earth, the irradiance (the total incident power per unit area) of the sun falling on the earth's atmosphere (solar constant = 1360 Wm^{-2}) varies over the year as the earth rotates around the sun. Solar radiation exists over a broad wavelength range with maximum radiative flux sharply centered in the visible region near 0.5 μm. As shown in Figure 2.4, the pronounced range of solar radiation include ultraviolet radiation (0.001 - 0.4 μm), visible radiation (0.4 - 0.7 μm) and infrared radiation (0.7 -100 μm). Most of the remote sensing instruments operate in the visible and near infrared range.

The earth surface emits and reflects (albedo) part of the solar energy, this gives the earth its brightness. The total radiation outside the earth surface (solar irradiance and earth's radiance) can be remotely sensed, the remotely observed radiation carries spectral and spatial information.

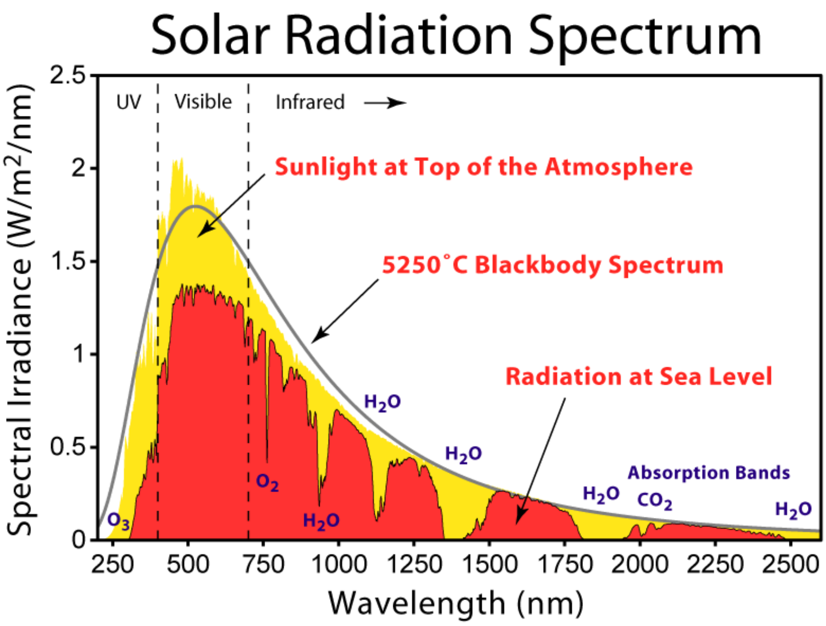

Figure 2.4: Solar spectrum [Credit: Wikimedia; Betacommand]

Figure 2.4 shows the spectrum of the sun as observed at the top of the atmosphere, at sea level, and as blackbody spectrum at sun-earth distance. The spectral range shown is 250 - 2500 nm, the figure shows $\approx 96.3\%$ of the total irradiance in the short wavelength region and the remaining $\approx 3.7\%$ at longer wavelengths.

Chapter 3

Instrumentation

3.1 European Remote sensing Satellite Two

There are several earth observation satellite in space. The satellite of interest here is the European Remote sensing Satellite two (ERS-2), which was launched in 1995 by the European Space Agency and ended in 2011. The ERS-2 was launched into a near-polar sun-synchronous orbit, at an average altitude of 795 km with an equator crossing time of 10:30 a.m for the descending node and with a repeat cycle of 35 days and an orbital period of about 100 minutes [Bednarz 1995]. On board of ERS-2 are the following earth observation instruments [Bednarz 1995]

- AMI-SAR: Active Microwave Instrument-Synthetic Aperture Antenna
- RA: Radar Altimeter
- PRARE: Precise Range And Range-rate Equipment
- **ATSR-2**: Along-Track Scanning Radiometer two
- **GOME**: Global Ozone Monitoring Experiment

Since an intercomparison of top of the atmosphere reflectance measured by GOME and ASTR-2 is to be carried out, this chapter focus on both instruments. Therefore a short description of both instruments and how they take measurements are discussed.

3.2 Description of GOME

The Global Ozone Monitoring Experiment [Burrows et al.,1999] (GOME) instrument is a UV - VIS (240 nm - 790 nm) spectrometer that measures solar irradiance and earthshine radiance. The GOME instrument scans across-track; in nadir and sideways (east to west), allowing radiation to be channeled into the instrument via a nadir scanning mirror. The instantaneous field of view is $29^o \times 0.14^o$ [Burrows et al.,1999]. In the Earth scanning mode, one scan cycle of GOME has an integration time of 6 seconds, 4.5 seconds for the forward scan, which makes up three GOME ground pixels (east, nadir and west) that covers approximately 320 km $\times$ 40 km of area each and 1.5 seconds integration time for the fly-back scan (which is three times faster) covering approximately 960 km $\times$ 40 km. Global coverage by GOME is achieved after 43 orbits (3days). The optical parameters of GOME instrument are shown in Table 3.1. The light that enters GOME

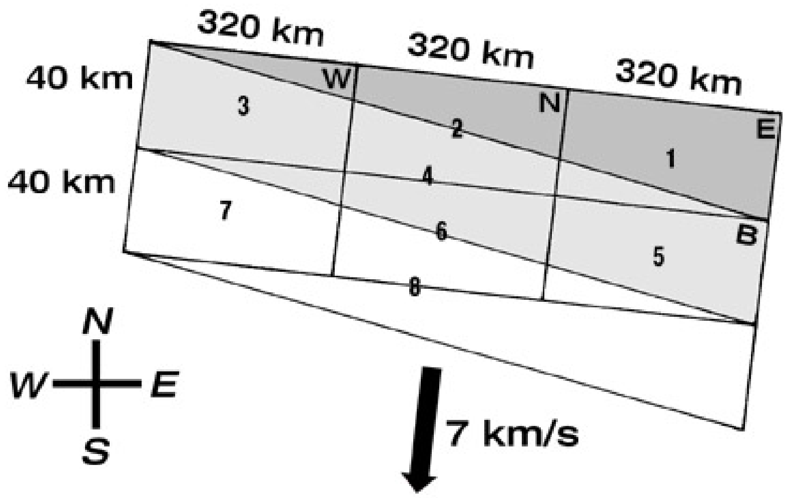

Figure 3.1: GOME nadir scan geometry [Credit: iup.uni-bremen.de]

through the scanning mirror is separated into four different spectral channels by a predisperser prism, a channel separator and a beam splitter to enable broad spectral coverage (between 240 nm and 790 nm) with a spectral resolution between 0.2 nm and 0.4 nm. For all spectral channels, the light is further separated by a diffraction grating and focused onto a linear Reticon diode array consisting of 1024 detector pixels. GOME is a polarization sensitive instrument and polarization measurement devices (PMDs) are added to the instrument for correcting the effects caused by the polariza-

Table 3.1: Table showing optical parameters of GOME [Burrows et al.,1999]

Channel	Wavelength [nm]	Integration time [sec]	Spectral resolution [nm]
1A	237 - 283	12	0.2
1B	283 - 316	1.5	0.2
2	311 - 405	1.5	0.17
3	**406 - 611**	1.5	0.29
4	**595 - 793**	1.5	0.33

tion sensitivity of the GOME instrument. The PMDs are three fast broadband silicon diode which measure polarized light covering the spectral ranges 300 - 400nm, 400 - 500nm, and 580 - 750nm. GOME measurements and retrieval objectives are grouped into

- Trace gas retrievals
- Clouds
- Radiation measurements
- Solar UV irradiance variability
- Aerosols
- Surface properties

3.2.1 GOME observation modes

GOME has three categories of observation modes namely, earth observation modes, calibration modes, and others modes.

1. Earth observation modes: the earth is in the field of view of the instrument and usually used on the sunlit part of the orbit with the scan mirror in static or scanning mode. Thus different observations are obtained, depending on the orientation of the scanning mirror enumerated below

- Nadir scanning
- North polar scanning
- South polar scanning
- Nadir static
- other static

2. Calibration modes: Instrument calibration is acquired also in different modes, the different modes are selected by the scan mirror position. Once every day, sun is observed by the instrument as the scan mirror points towards the sun diffuser. All internal sources are switched off and the solar port is open. Other calibration modes are:

   - Moon: the scan mirror points towards the moon at viewing angels of +70^o to +85^o.
   - LED: the scan mirror points towards the GOME telescope, the instrument solar port is closed and the LEDs are switched on.
   - Dark: the scan mirror points towards the GOME telescope, all internal light sources switched off and the solar port is closed.

3. Other modes: these modes are mainly used for instrument maintenance or transitory states. Data packet generated in these modes contain less information.

3.3 Description of ATSR-2

Along Track Scanning Radiometer two (ATSR-2) is an imaging radiometer that measures the amount of light traveling through the atmosphere in two different angles. It carries out conical scans that permit two different observations at the same scene with differing atmospheric path within a short time interval ($\approx$ 150 sec.). The instrument observes solar irradiance and earth's radiance at a 55^o viewing angle along track (forward scan) then observing the same scene at an angle close to the nadir. The viewing geometries produce two 500 km wide curve swaths; the forward swath and the nadir swath are 900 km apart at the surface. The forward nadir swaths contains 371 and

555 pixels across track, respectively (Fig.2.2). The nominal instantaneous field of view pixel size is 1 km^2 at the center of the nadir and 1.5 km $\times$ 2km at the center of the forward swath [Mutlow et al.,1999]. Unlike ATSR-1, ATSR-2 has seven channels, three in the visible region centered at 0.555, 0.659, and 0.865 μm and four channels in the infrared region centered at 1.6, 3.7, 10.85, and 12 μm. Table 3.2 shows the spectral bands of ATSR-2 instrument. The visible channels of ATSR-2 have excellent radiometric per-

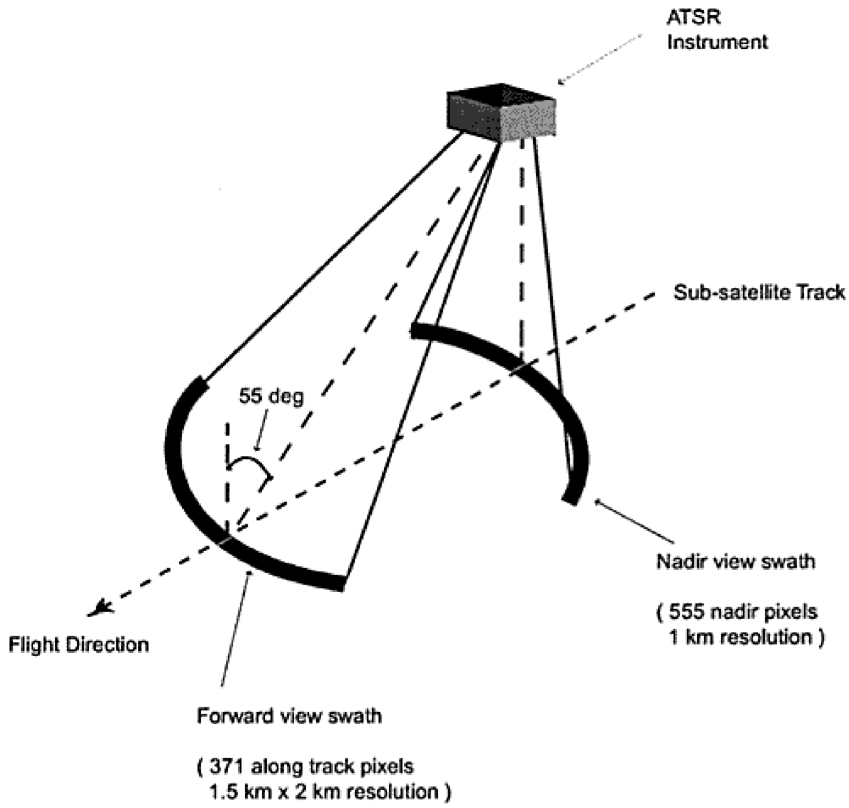

Figure 3.2: ATSR-2 scan geometry [Credit: earth.esa.int]

formance and it is normalized by observing the sun once every day, also the infrared channels is calibrated by scanning a blackbody calibration target [Mutlow et al.,1999]. However ATSR-2 instrument has been carefully designed and thoroughly calibrated before launch, to sustain it's high calibration standard.

The direct measurement of atmospheric effect is obtained by combining the data from the forward and nadir scan, which gives an atmospheric correction for the surface data set [Mutlow et al.,1999]. ATSR-2 is a multipurpose imaging radiometer which is used to retrieve a number of measurements, with emphasis on very accurate sea surface temperature. Some of the variables retrieved by ATSR-2 are

- Sea surface temperature
- Sea-ice cover
- Aerosol volcanic ash (Total column)
- Land surface temperature
- Cloud optical depth
- Cloud cover
- Aerosol type

Table 3.2: Table showing ATSR-2 optical parameters [Stricker et al.,1995]

Band	Band center [μm]	Band width [μm]
1	3.7	20
2	10.8	20
3	12	20
4	**0.555**	**20**
5	**0.659**	**20**
6	0.865	20
7	1.61	20

Chapter 4

Intercomparison Method

4.1 Data

The intercomparison of newly processed GOME level 1b Nadir reflectance spectra Version 5, available from January 1997 to December [Burrows et al.,1999] with ATSR-2 gridded reflectance data available from 1995 to 2003 (resampled to 1 km $\times$ 1 km) [North et al.,1999] is be carried out. Cloud fraction information derived from ATSR-2 [Sayer et al.,2011] is used to separate ground scenes into cloudy and cloud-free scenarios. Furthermore, the TEMIS LER (Lambertian Equivalent Reflectivity) climatology database [Koelemeijer et al.,2003] is used to further subdivide the GOME cloud free ground scenes into dark and bright scenarios. Only the nadir pixel measurements of the GOME and ATSR-2 are considered for the reflectance validation, since only the GOME nadir pixel overlaps completely with the ATSR-2 footprint. In figure 4.1, GOME pixels are in blue (west), green (nadir), yellow (east), and purple (backscan). ATSR-2 footprint in black.

4.1.1 GOME data

The optical components of GOME has suffered degradation during its observatory period. By the daily observation of the sun irradiance, a complete record of GOME degradation is recorded. Thus a *correction factor* (assuming that sun may serve as a stable reference) can be used to correct the sun irradiance and can also be applied to the

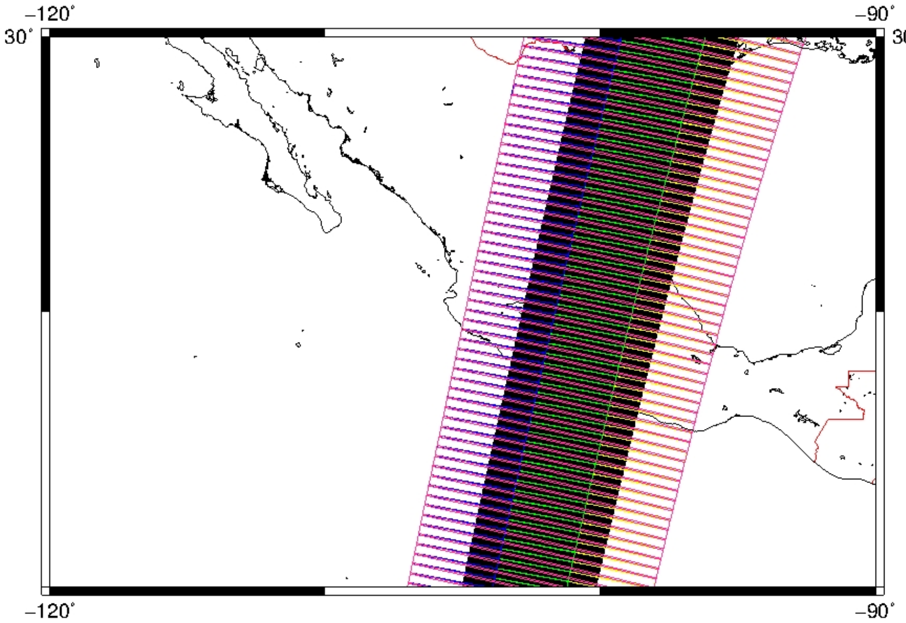

Figure 4.1: Main differences between GOME and ATSR-2 swath. GOME pixels are in blue (west), green (nadir), yellow (east), and purple (backscan). ATSR-2 footprint in black. [Credit: Stefan Boetel pers-com]

radiance [Tilstra et al.,2006]. However the correction factor when applied to the solar irradiance and earth radiance cancel out when calculating reflectance from equation 4.1.

Calibrated earthshine radiance and solar irradiance spectra of GOME level 1 products are provided by the European Space Agency (ESA) with a GOME data processor (DLR/DFD). The level 1 data product includes header, fixed calibration data, ground pixel, specific calibration parameters, and GOME science data in different spectra bands. The GOME channels 1 and 2 are subdivided into two independent channels 1a, 1b and 2a, 2b respectively with different integration times, the integration time for all channels are increased for high zenith angles.

The newly processed GOME-1 level 1 nadir measurement (version 5 without considering correction factor of instrument degradation) of band 3 and 4, with an integration time of 1.5 second for both bands has been used in this validation study.

4.1.2 ATSR-2 gridded reflectances

The ATSR-2 nadir scan gridded reflectance [North et al.,1999] resampled to 1km $\times$ 1km has been used in for this work. The ATSR-2 level 1b products data was extracted online from the ATSR online archive.

ATSR-2 data is processed using SADIST (Synthesis of ATSR Data Into Sea-surface Temperatures), the Rutherford Appleton Laboratory's ATSR data-processing scheme [Zavody et al.,1994]. The SADIST ATSR-2 product set is made up of

1. Ungridded products: contain nadir and forward pixel records that are not collocated
2. Gridded products: contain collocated nadir and forward pixel records
3. Spatially-averaged products: contain data which have been averaged spatially

For scientific use usage of the ATSR-2 data, the spatial view difference and scan geometry of ATSR-2 is removed in the data processing by the derivation of the earth location of the acquired pixels (geolocation) and spatially matching the nadir and forward views (view collocation). The geolocation proceeds by mapping the curved swaths onto an equidistant grid of 512 $\times$ 512 km^2 with a 1 km spacing [Mutlow et al.,1999].

4.1.3 GRAPE cloud parameters

GRAPE cloud parameters data base derived from ATSR-2 measurements contains different cloud properties data. The GRPAE cloud fraction has been used to separate the derived GOME reflectance into cloudy and cloud free scenes. The GRAPE products are internally flagged as show Table 4.1, as different threshold depends on the use of data.

Table 4.1: Table quality control information [Sayer et al.,2010]

Variable name	Description	valid range
Flag	Flag to indicate type of data	1 = cloud 2 = aerosol 3 = no data
Total cost	Cost indication of forward model fit to measurements given the solution	positive real
Iterations	Number of iterations the retrieval took to converge	-1 - 25
Retrieval quality flag	Flag to be used as indication of retrieval quality 0: Failed to converge, or very poor fit 1: Poor fit 2: Moderate fit 3: High quality fit	0 - 3

4.1.4 TEMIS LER climatology data

The Lambert-equivalent reflectivity is the value of the Lambertian spectral surface albedo for which the measured reflectivity at the top of the atmosphere are equal [Koelemeijer et al.,2003]. A global database of Lambert-equivalent reflectivity of the earth's surface derived from the top of atmosphere reflectivity measured by GOME has been constructed by [Koelemeijer et al.,2003]. The database values at 555 nm and

Table 4.2: Table of wave length in the TEMIS LER database [Koelemeijer et al.,2003]

wavelength [nm]	Retrieval application
335.0	Ozone (Huggins band)
380.0	Aerosol
416.0	Aerosol
440.0	NO_2
463.0	O_2 - O_2
494.5	Aerosol
555.0	vegetation
610.0	Aerosol
670.0	Cloud detection
758.0	O_2 (A band)
772.0	O_2 (A band)

670 nm have been used in this work to separate the cloud free pixels into bright and dark pixels using a threshold value as mentioned in section 4.2.

4.2 Validation method

[1] The nadir observation for GOME and ATSR-2 available from July 1997 to 2002 are used for in this validation work, i.e only the July and January data are used for seasonal variability investigation. The following steps are taken in analysis of the data.

[1] Ideas: from SCILOV-10 VIS reflectance validation method

For a first step: the reflectances measured by both instruments are derived for each spectral band where GOME bands (3 and 4) overlaps with ATSR-2 bands (4 and 5) centered at 555nm and 659nm respectively. Since both instruments measure solar irradiance E_0 and earthshine (radiance) at the top of the atmosphere, the reflectance R at the top of the atmosphere is calculated from

$$R = \frac{\pi I}{E_0 \mu_0} \tag{4.1}$$

here μ_0 is the cosine of the solar zenith angle θ_0.

The spectrally averaged GOME reflectances are derived by integrating over ATSR-2 bandwidth of 20 nm, followed by deriving the spatially averaged ATSR-2 reflectances by integrating over ATSR-2 pixels that fall inside the GOME footprint. GRAPE cloud fraction data is used subdivide the GOME pixels into cloudy and cloud free pixels, the GOME-1 TEMIS LER climatology data containing surface spectral albedo at 555nm and 670nm are used to further subdivide the GOME pixels with corresponding into bright and dark pixels.

In the second Step: Evaluation of general statistics; the linear relation between the spectrally averaged GOME and spatially averaged ATSR-2 reflectances for the different pixels scenarios are investigated

- All ground pixels
- Cloudy pixels (CF $>$ 0.98)
- Cloud free pixels (CF $<$ 0.2): further separated into *Dark* (surface spectral albedo $<$ 0.2)and *Bright* (surface spectral albedo $>$ 0.2) pixels

using a linear regression model below in equation 4.2

$$R_A(\lambda) = M \times R_G(\lambda) + B \tag{4.2}$$

here R_A is averaged collocated ATSR-2 reflectance, R_G is averaged GOME reflectance,

M is slope, and B is Intercept.

The relative difference between the reflectance of both instruments is derived using the relation below

$$R.d = 100 \times \frac{R_G - R_A}{R_A} \tag{4.3}$$

Also to see whether the GOME calibration reflectance is changing over ESR-2 observation period, time series analysis of the derived slope (M), intercept (B) and correlation coefficient from equation 4.2 over the 8 years period (July 1997 to July 2002) for July and January data are investigated. This is done by applying a linear regression model

$$y = m.x + b \tag{4.4}$$

here y is the slope (M), intercept (B), and correlation coefficient (R) from equation 4.2. Also x is the time in months. Thus only two GOME channels are (channel 3: 405 - 611 nm and channel 4: 595 - 793 nm) can be investigated using this validation method.

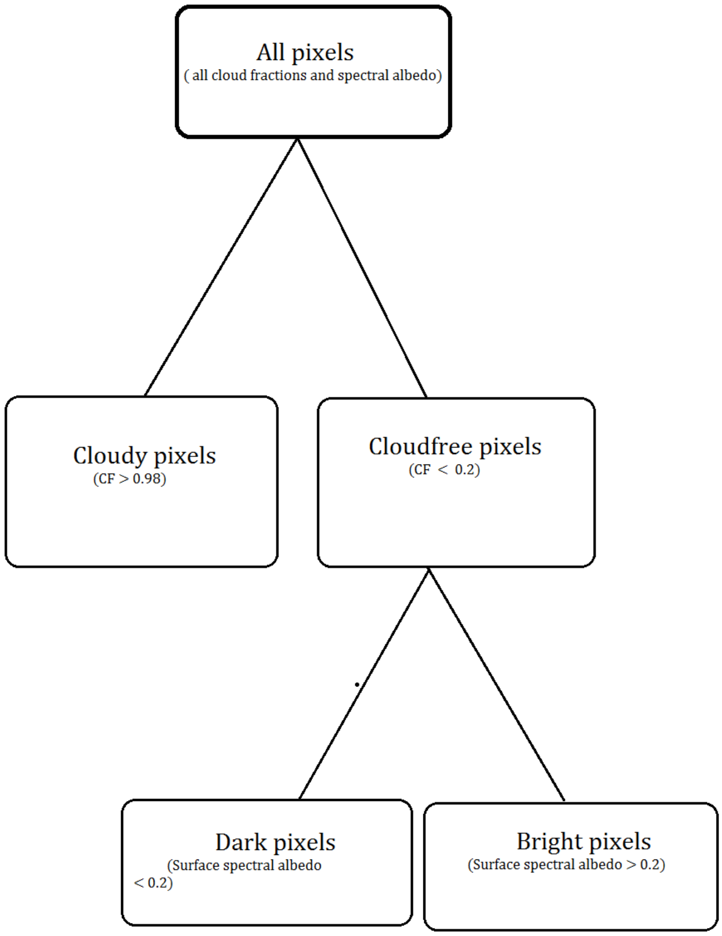

Figure 4.2: Schematic representation of the GOME ground pixels separation into different scenarios using GRAPE cloud parameter and TEMIS LER spectral surface albedo values.

Chapter 5

Result and Analysis

The main aim of this work is to carry out an intercomparison between GOME and ATSR-2 TOA reflectances at 555 nm and 659 nm using data from 1996 to 2003. GOME lost the global coverage in July 2003 due to malfunction of the internal tape recorder and the retrieval quality of the cloud fraction for 1996 from ATSR-2 is consistently bad because they were using the wrong channels. Thus data for 2003 and 1996 are ignored in this validation work.

The method as described in section 4.2 is used in the intercomparison by following two approaches. In this intercomparison analysis the radiometric degradation of the instrument is not taking into account, i.e correction factor in the GOME-1 processor is neglected.

5.1 Monthly gridded data

First, monthly gridded data sets separated into four different scenarios (all data, cloudy scene, dark scene, and bright scene) were created using cloud fraction and spectral surface albedo information. Figure 5.1 and 5.2 show GOME spectrally averaged reflectances for all ground pixels (considering all cloud fractions and surface spectral albedo) at 555 nm and 659 nm measured in January 1997 and July 1997. Figure 5.3 and 5.4 show color coded scatter plots of spectrally averaged GOME (x-axis) and spatially averaged ATSR-2 reflectances (y-axis). The slope (M) and intercept (B) and correlation coefficient is calculated using the linear regression model. For January 1997 a very

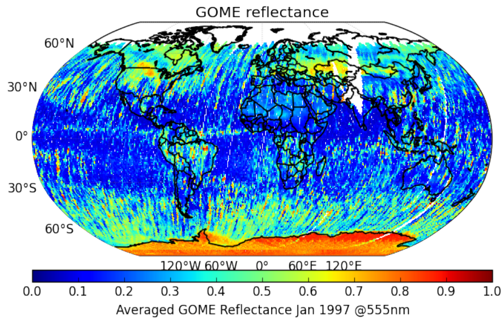

Figure 5.1: Monthly gridded GOME reflectances at555 nm and 659 nm for January 1997 considering all cloud fraction and spectral surface albedo values.

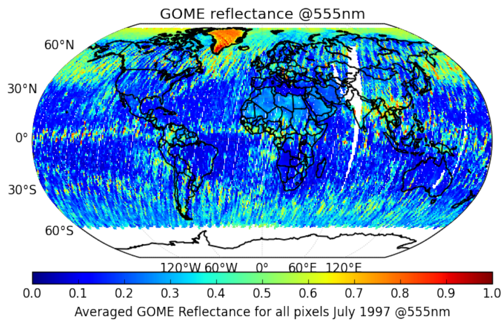

Figure 5.2: Monthly gridded GOME reflectances at 555 nm and 659 nm for July 1997 considering all cloud fraction and spectral surface albedo values.

high correlation coefficient of $\sim 94\%$ and an overestimation of GOME reflectance in the visible of 11% at 555 nm and 659 nm, with intercepts far less than one. For July 1997 a very good correlation coefficient of $\sim 89\%$ and a overestimation of GOME reflectance of $\sim 12\%$ at both wave lengths, also with intercepts far less than one.
Table 5.1 and 5.2 show the linear regression parameters for all scenarios: cloudy, dark and bright ground pixels at 555nm and 659nm for January and July 1997. From the tables below we observe good statistics for All ground pixels, cloudy, and bright pixels for both months (January and July 1997) and at both wavelengths. A very poor

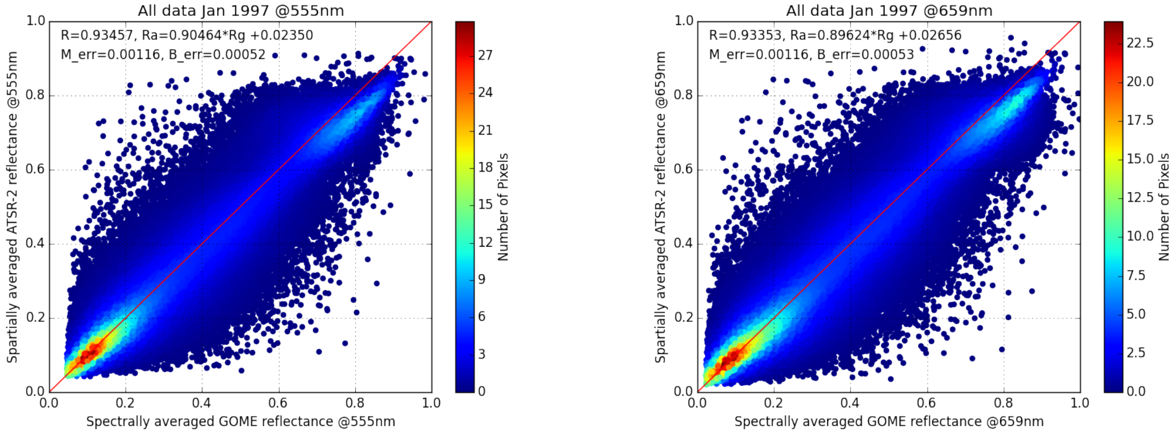

Figure 5.3: Scatter plots between spectrally averaged GOME and spatially averaged ATSR-2 reflectances at 555nm and 659nm for January 1997 considering all cloud fraction and spectral surface albedo values. After applying linear regression model (from equation 4.2)slope M = 0.90464±0.00116, intercept B = 0.02350±0.00052, and corr. coefficient R = 0.93457 at 555nm. At 659nm slope M = 0.89624±0.00116, intercept B = 0.02656±0.00053, and corr. coefficient R = 0.93353. The color bars show the number of pixels

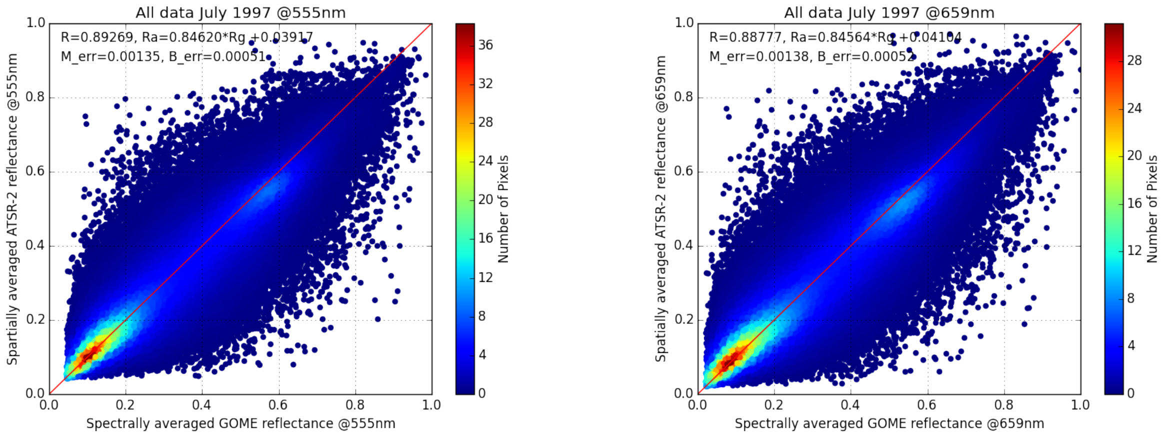

Figure 5.4: Scatter plots between spectrally averaged GOME and spatially averaged ATSR-2 reflectances at 555nm and 659nm for July 1997 considering all cloud fraction and spectral surface albedo values. At 555nm slope M = 0.84620±0.00135, intercept B = 0.03917±0.00051, and corr. coefficient R = 0.89269. At 659nm slope M = 0.84564±0.00138, intercept B = 0.04104±0.00052, and corr. coefficient R = 0.88777.

statistics for the dark ground pixels also for both months and at both wavelengths respectively.

Table 5.1: Table showing linear relation parameters for January 1997

Scene	Slope [M] 555 nm	Intercept [B] 555 nm	Slope [M] 659 nm	Intercept [B] 659 nm
All pixels	0.9046±0.0012	0.0235±0.0005	0.8962±0.0012	0.0266±0.0005
Cloudy pixels	0.9323±0.0051	0.0124±0.0030	0.9306±0.0050	0.0137±0.0030
Dark pixels	0.5438±0.0170	0.0283±0.0170	0.6023±0.0173	0.0166±0.0021
Bright pixels	0.8239±0.0846	0.0249±0.0279	0.8045±0.0913	-0.0097±0.0316

Table 5.2: Table showing linear relation parameters for July 1997

Scene	Slope [M] 555 nm	Intercept [B] 555 nm	Slope [M] 659 nm	Intercept [B] 659 nm
All pixels	0.8462±0.0014	0.0392±0.0005	0.84564±0.0014	0.0410±0.0005
Cloudy pixels	0.9373±0.0120	0.0209±0.0058	0.9482±0.0121	0.0215±0.0059
Dark pixels	0.5801±0.0133	0.0359±0.0016	0.6522±0.0115	0.0257±0.0013
Bright pixels	1.0224±0.0553	-0.0702±0.0191	0.8900±0.0626	-0.0508±0.0206

5.2 Relative difference and Error

Relative difference between the spectrally averaged GOME reflectances and spatially averaged ATSR-2 reflectances is derived by applying equation 4.3 to all pixels. Monthly averaged relative difference has been derived for all scenarios (cloudy, dark, and bright scenes). From the mean relative difference obtained for January and July 1997 data, positive mean relative difference is derived for all scenarios at 555nm and 659nm. From the mean relative differences, it shows that spectrally averaged GOME reflectances is systematically higher than spatially averaged ATSR-2 reflectances. Considering all cloud fraction and spectral surface albedo at 555nm relative difference is 7.9% and 8.8% at 659nm respectively for January 1997 and 7.4% at 555nm and 7.2% 659nm for July 1997.

The most probable cause of the derived relative difference could be due to different radiometric calibration accuracy of both instruments. The designed accuracy of 2% for the ATSR-2 reflectivity measurement [RAL 1996] and 3.5% for the GOME earthshine radiance and solar irradiance measurements [Bednarz 1995]. Also both instruments are normalized by observing the sun once in a day. The sun is observed through the calibration units which differs for both instruments, hence the optical path through each instrument in the solar observation mode differs [Koelemeijer et al.,1998].

GOME optical components are subject to degradation. From the daily measurements of the solar irradiance, a complete record the instrument degradation is obtained. The solar irradiance and earth radiance are corrected using the obtained record. Studies on GOME UV reflectivity degradation [Tanzi et al.,2001] show that generally the solar irradiance measurements is likely to degrade faster than the earth's irradiance measurements, leading to an artificial increase of reflectivity with time [Koelemeijer et al.,2003]. However the GOME-1 version 5 data used in this work does not fully account for the radiometric degradation of the GOME instrument.

5.3 Time series analysis

In second step how GOME calibration reflectance is changing over time (from 1997 to 2002) is investigated. Seasonal time series analysis (January and July data) of slope, intercept, and correlation coefficient derived from equation 4.2 is performed and a linear regression model using equation 4.4 is applied afterword.

Figure 5.5 shows the time series data (considering all cloud fraction and spectral surface albedo) investigating how the GOME reflectance calibration is changing from January 1997 to December 1997 at 555nm and 659nm. Poor statistics are offered by

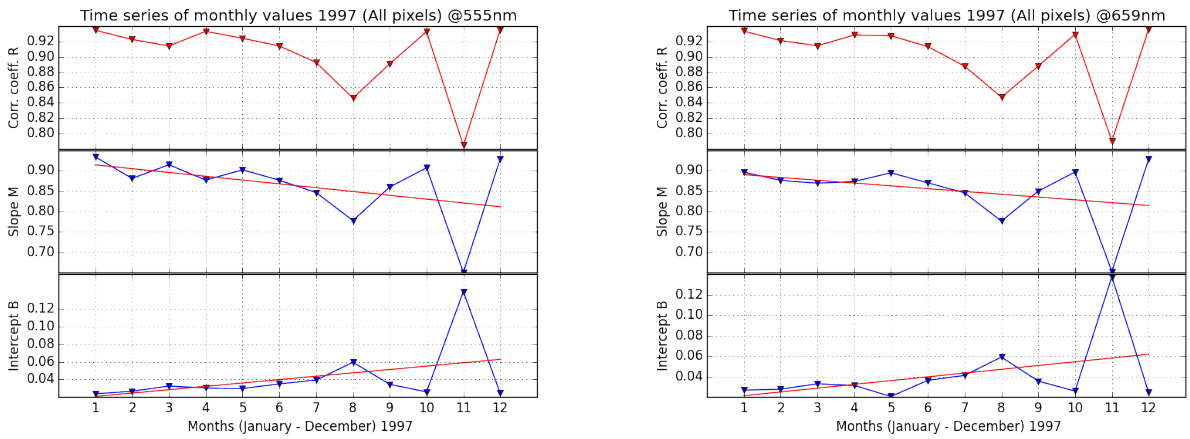

Figure 5.5: Time series of monthly GOME values of slope (M), intercept (B), and correlation coefficient (R) considering all cloud fraction and surface spectral albedo values at 555 nm and 659 nm from January to December 1997.

November 1997 data and August 1997 relative to the rest of the months at both wavelengths. This investigation is carried out for all scenarios, see Appendix for similar plots representing other scenarios. The linear regression regression base on time series data (January - December 1997) of slope (M) and intercept (B) for all scenarios derived using equation 4.4 are shown in Table 5.4. Table 5.4 below shows value for slope (m) and intercept (b) derived from the seasonal (January and July) time series from 1997 - 2002 base on slope (M), intercept (B) and correlation coefficient (R) at 555 nm and 659 nm.

Table 5.3: Table summarizing the linear relation parameters based on time series data of slope (M) and intercept (B) derived from Equation 4.4 for 1997 (January-December) dataset.

Slope M		555 nm	659 nm
All pixels	b	0.9234±0.0514	0.8497±0.0494
	m	-0.0931±0.0070	-0.0068±0.0067
Cloudy pixels	b	0.9336±0.0334	0.9206±0.0097
	m	-0.0017±0.0045	0.0022±0.0013
Dark pixels	b	0.0558±0.0494	0.5826±0.0444
	m	0.0134±0.0067	0.0111±0.0060
Bright pixels	b	0.693±0.1181	0.8412±0.1564
	m	0.0244±0.0161	-0.0011±0.0058
Intercept B		555 nm	659 nm
All pixels	b	0.0167±0.0212	0.0175±0.0209
	m	0.0038±0.0029	0.0037±0.0028
Cloudy pixels	b	0.0170±0.0070	0.0192±0.0071
	m	0.0006±0.0010	0.0003±0.0010
Dark pixels	b	0.0306±0.0066	0.0213±0.0046
	m	-0.0008±0.0009	-0.0004±0.0006
Bright pixels	b	0.0867±0.0427	-0.0022±0.0467
	m	-0.011±0.0058	0.0005±0.0064

Table 5.4: Table summarizing the linear relation parameters based on time series data of slope (M) and intercept (B) derived from Equation 4.4 for January and July (from 1997 - 2002) dataset.

Slope M		555 nm	659 nm
All pixels	b	0.9474±0.0990	0.96093±0.1788
	m	-0.0137±0.0135	-0.0222±0.0243
Cloudy pixels	b	0.8892±0.4311	1.1195±0.1753
	m	0.0488±0.0586	-0.0225±0.0238
Dark pixels	b	0.6438±0.0642	0.6755±0.1666
	m	-0.0014±0.0087	-0.0043±0.0226
Bright pixels	b	0.6709±0.3714	2.4708±4.5889
	m	0.0324±0.00505	-0.5731±0.6235
Intercept B		555 nm	659 nm
All pixels	b	0.0190±0.0294	0.3346±0.0080
	m	0.0033±0.0040	-0.0009±0.0011
Cloudy pixels	b	0.0624±0.01631	-0.0633±0.1506
	m	-0.0189±0.0022	0.0110±0.0205
Dark pixels	b	0.0237±0.0097	0.0230±0.0061
	m	-0.0010±0.0013	-0.0012±0.0008
Bright pixels	b	0.0230±0.1308	-0.6030±1.6460
	m	-0.0015±0.0178	0.2053±0.2237

Chapter 6

Conclusion and Summary

An intercomparison study between GOME and ATSR-2 reflectances measured at the top of the atmosphere on board ESR-2 base on January and July dataset from 1997 to 2002 is presented. The new version 5 GOME-1 level1 data (without considering the correction factor in the GOME processor) is used for this study. ATSR-2 is a highly calibrated instrument with a calibration accuracy of 2%, and GOME is a well calibrated instrument with calibration accuracy between 3 - 3.5%. The GOME-1 reflectances were spectrally averaged by integrating over the ATSR-2 bandwidth (20 nm) at 555 nm and 659 nm. Also the ATSR-2 reflectances were spatially averaged by integrating over the GOME foot print. The reflectances have been subdivided into different scenarios as cloudy and cloud free scenes base on cloud fraction and surface spectral albedo values. Time series analysis of the slope (M), intercept (B), and correlation coefficient (R) for January and July data from 1996 - 2003 at 555 nm and 659 nm was carried out for all scenarios.

It has been demonstrated in this work that there is a slight disagreement of the GOME measurements (using GOME-1 version 5 data) with the highly calibrated ATSR-2 measurements considering all scenarios (all data, cloudy, and cloud free data), the measured ATSR-2 TOA reflectance is systematically lower than that of GOME. From the slope time series GOME overestimates the top of the atmosphere reflectance on average by approximately 11% at both wavelengths. Thus from the result of the validation study, we confirm that the GOME provide measurement of top of atmosphere reflectance with lesser accuracy (10%) compared to ATSR-2. However GOME is a well calibrated instrument, it is suitable for the retrieval of atmospheric species (Trace gases, clouds, aerosols) and earth surface properties.

6.1 Outlook

It will be convenient to carry out thesame intercomparison study using other GOME processor versions (e.g using GOME-1 version 4 data or other versions that take into account the correction factor), by applying thesame validation method as applied in this work.

Bibliography

[Stricker et al.,1995] Stricker, N. C. M., Hahne, A., Smith, D. L., Delderfield, J., Oliver, M. B., and Edwards, T. (1995). ATSR-2: The evolution in its design from ERS-1 to ERS-2. Esa Bulletin,1, 32-37.

[Bednarz 1995] Bednarz, F. (1995). GOME Global Ozone Monitoring Experiment users manual. In ESA Special Publication (Vol. 1182).

[Burrows et al.,1999] Burrows, J. P., Weber, M., Buchwitz, M., Rozanov, V., Ladstätter-Weißenmayer, A., Richter, A., ... and Perner, D. (1999). The global ozone monitoring experiment (GOME): Mission concept and first scientific results. Journal of the Atmospheric Sciences, 56(2), 151-175.

[Wallace and Hobbs 2006] Wallace, J.M., and Hobbs, P.V.,(2006). Atmospheric Science: An Introductory Survey (vol. 92), Academic Press. Page-10

[Kokhanovsky et al.,2008] Kokhanovsky, A. A., Schreier, M., and von Hoyningen-Huene, W. (2008). The comparison of spectral top-of-atmosphere reflectances measured by AATSR, MERIS, and SCIAMACHY onboard ENVISAT. Geoscience and Remote Sensing Letters, IEEE, 5(1), 53-56.

[Arino et al.,199] Arino, O., and Rosaz, J. M. (1999). 1997 and 1998 world ATSR fire atlas using ERS-2 ATSR-2 data. In Proc. Joint Fire Sci. Conf (pp. 177-182). Boise, ID.

[North et al.,2008] North, P., Brockmann, C., Fischer, J., Gomez-Chova, L., Grey, W., Heckel, A., ... and Regner, P. (2008, September). MERIS/AATSR synergy algorithms for cloud screening, aerosol retrieval and atmospheric correction. In Proc. 2nd MERIS/AATSR User Workshop, ESRIN, Frascati (pp. 22-26).

[Tilstra et al.,2006] Tilstra, L. G., and Stammes, P. (2006). Intercomparison of reflectances observed by GOME and SCIAMACHY in the visible wavelength range. Applied optics, 45(17), 4129-4135.

[Koelemeijer et al.,1998] Koelemeijer, R. B. A., Stammes, P., and Watts, P. D. (1998). Comparison of visible calibrations of GOME and ATSR-2. Remote Sensing of Environment, 63(3), 279-288.

[Koelemeijer et al.,1999] Koelemeijer, R. B. A., and Stammes, P. (1999), Effects of clouds on ozone column retrieval from GOME UV measurements, J. Geophys. Res., 104, 8281–8294.

[Koelemeijer et al.,2003] Koelemeijer, R. B. A., De Haan, J. F., and Stammes, P. (2003). A database of spectral surface reflectivity in the range 335–772nm derived from 5.5 years of GOME observations. Journal of Geophysical Research: Atmospheres (1984–2012), 108(D2).

[Sayer et al.,2010] Sayer, A. M., Poulsen, C. A., Grainger, D. (2010). GRAPE output product version 3.2

[Sayer et al.,2011] Sayer, A. M., Poulsen, C. A., Arnold, C., Campmany, E., Dean, S., Ewen, G. B. L., ... and Watts, P. D. (2011). Global retrieval of ATSR cloud parameters and evaluation (GRAPE): dataset assessment. Atmospheric Chemistry and Physics, 11(8), 3913-3936.

[Aben et al.,20003] Aben, I., Tanzi, C. P., Hartmann, W., Stam, D. M., and Stammes, P. (2003). Validation of space-based polarization measurements by use of a single-scattering approximation, with application to the Global Ozone Monitoring Experiment. Applied optics, 42(18), 3610-3619.

[Tanzi et al.,2001] Tanzi, C.P., Snel, R. and Aben.I (2001). Degradation of observation in the UV of the Global Ozone Monitoring Experiment (GOME), in proceedings IRS-200: Current Problems in Atmospheric radiation, edited by W:L Smith and Y.M Timofeyev, pp. 181-184, A. Deepak Publ., Hampton.

[Mutlow et al.,1999] Mutlow, C. T., Murray, M. J., Bailey, P., Birks, A. R., and Smith, D. L. (1999). ATSR-1/2 user guide issue 1. ESA User Guide.

[RAL 1996] Rutherford Appleton Laboratory (RAL) (199a), ATSR-2 flight operation manual, ER-MA-RAL-AT-2001, RAL, Chilton Didcot, UK.

[Kokhanovsky et al.,2007] Kokhanovsky, A. A., Bramstedt, K., von Hoyningen-Huene, W., and Burrows, J. P. (2007). The intercomparison of top-of-atmosphere reflectivity measured by MERIS and SCIAMACHY in the spectral range of 443–865 nm. Geoscience and Remote Sensing Letters, IEEE, 4(2), 293-296.

[Schlundt et al.,2014] Schlundt, C., Noel, S., and Weber, M., Intercomparison study of top of atmosphere reflectances measured by SCIAMACHY and MERIS on board ENVISAT from August 2002 to March 2012, In preparation.

[Rozanov et al.,2006] Rozanov, V. V., Kokhanovsky, A. A., Loyola, D., Siddans, R., Latter, B., Stevens, A., and Burrows, J. P. (2006). Intercomparison of cloud top altitudes as derived using GOME and ATSR-2 instruments onboard ERS-2. Remote Sensing of Environment, 102(1), 186-193.

[Zavody et al.,1994] Zavody, A.M., Gorman, M.R., Lee, D.J., Eccles, D., Mutlow, C.T., and Llewellyn-Jones, D.T. The ATSR data processing scheme developed from the EODC, int. J. Remote sensing, 15, 827-843, 1994.

[North et al.,1999] North, P. R., Briggs, S., Plummer, S. E., and Settle, J. J. (1999). Retrieval of land surface bidirectional reflectance and aerosol opacity from ATSR-2 multiangle imagery. Geoscience and Remote Sensing, IEEE Transactions on, 37(1), 526-537.

[Briegleb et al., 1986] Briegleb, B.P., Miinnis, P., Ramanathan, V., and Harrison, E. (1986). Comparison of regional clear-sky albedos inferred from satellite observations and model computations. Journal of climate and Applied Meteorology 25:214-226.

[seos-project.eu,2015] SEOS (2015). Remote Sensing Using Laser. wwww.seos-project.eu

[Boettger et al.,2006] Böttger, U., Nieke, J., and Schlaepfer, D. (2006). Assessing polarization effects for the Airborne imaging spectrometer APEX. Advances in Radio Science, 4(10), 323-328.

[Coakley, J. A.,2003] Coakley, J. A. (2003). Reflectance and albedo, surface. Encyclopedia of the Atmosphere, JR Holton and JA Curry, eds.(Academic, 2003), 1914-1923.

[earth.esa.int] `http//:earth.esa.int/web/guest/data-access/browse-data-products`. Accessed 10.12.2015

[Baumann P.R.,2010] Baumann .P.R. (2010). Introduction to remote sensing. www.oneonta.edu

Appendix A

Additional plots

cloudy pixels

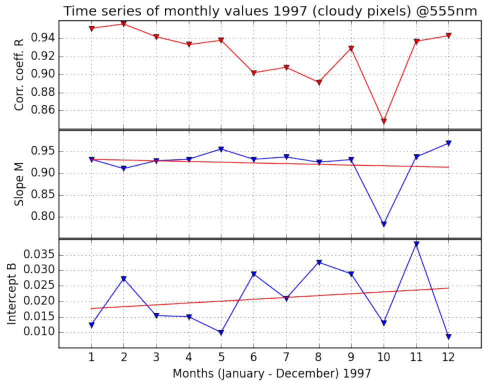

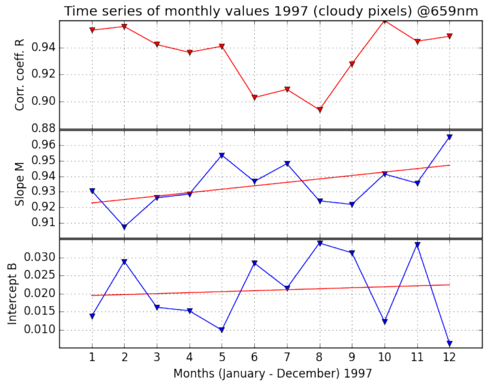

dark pixels

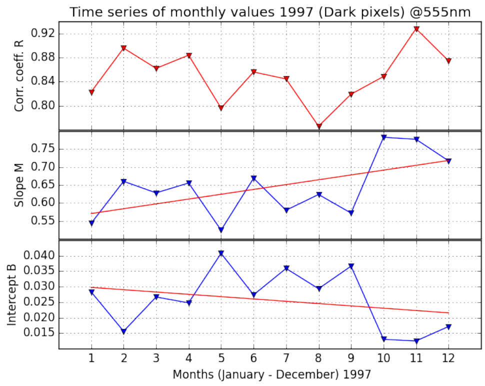

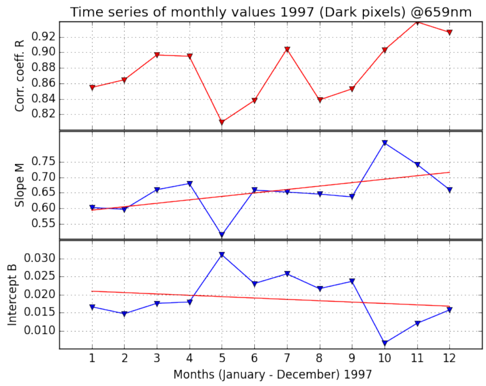

bright pixels

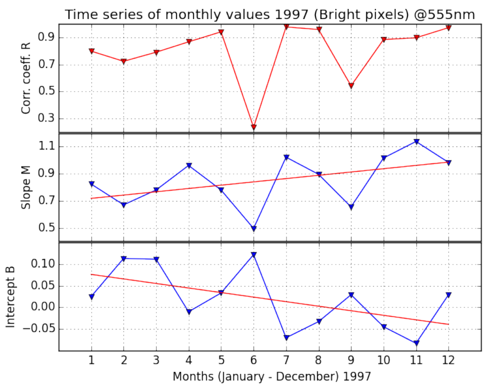

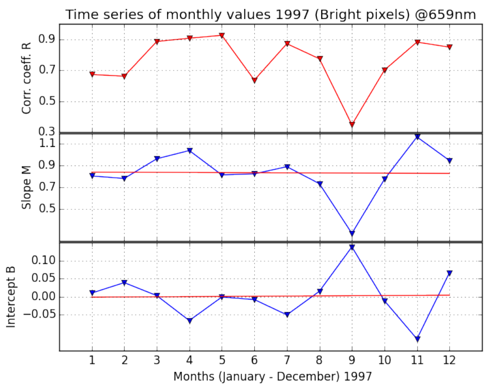

Figure A.1: Monthly (January - December) variations of Slope (M), Intercept (B), and correlation coefficient (R) for 1997 data at 555nm and 659nm for different pixel scenarios

winter

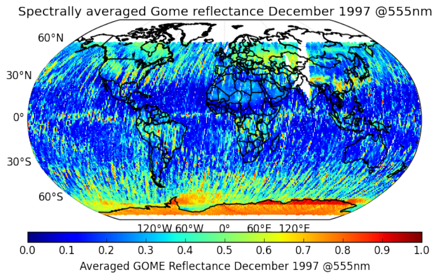

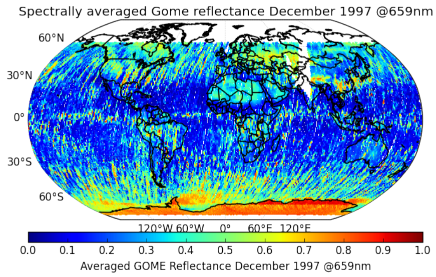

spring

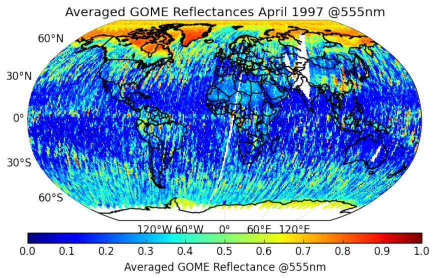

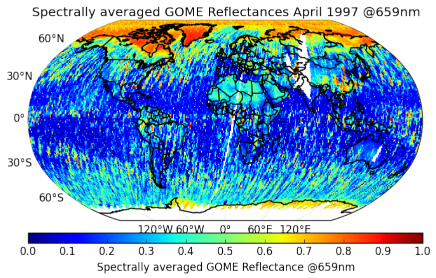

summer

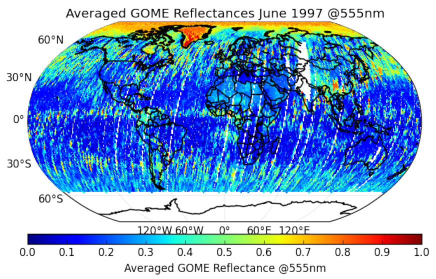

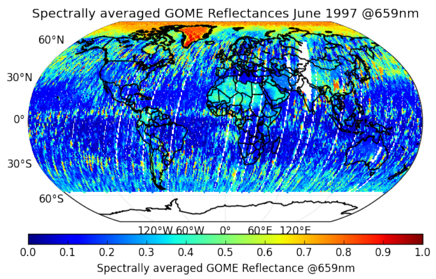

autumn

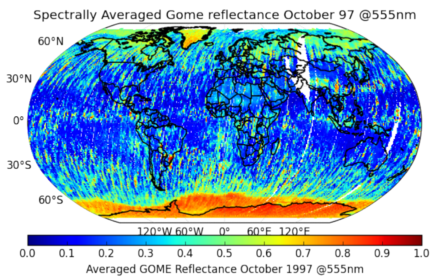

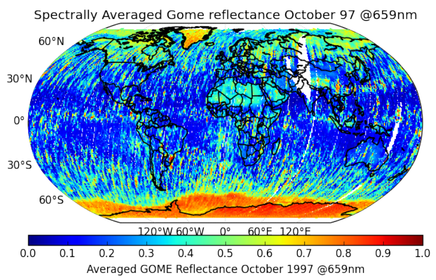

Figure A.2: Seasonal global map of spectrally averaged GOME reflectances at 555nm and 659nm for 1997 data

Cloudy pixels

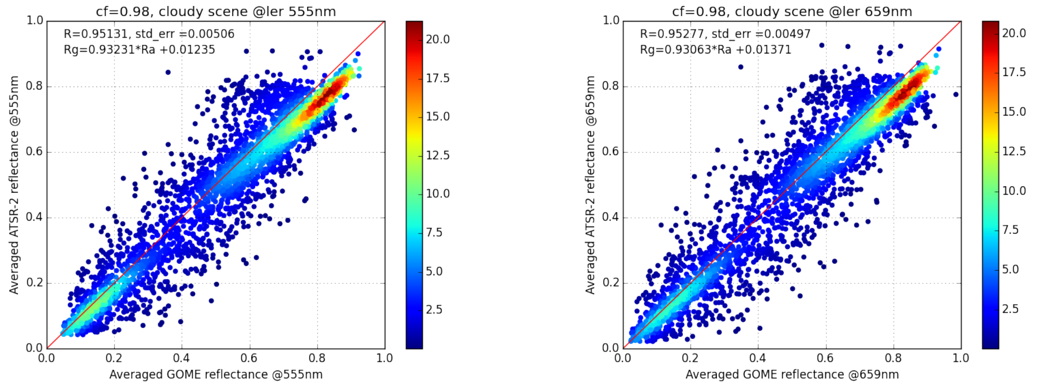

Dark pixels

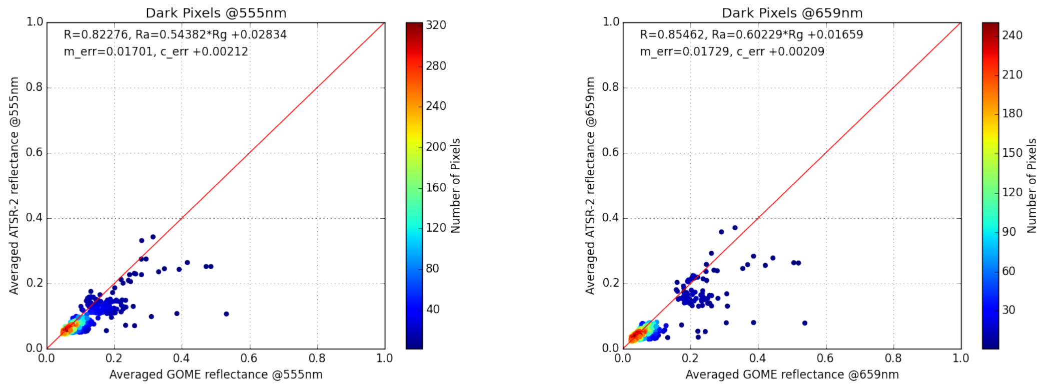

Bright pixels

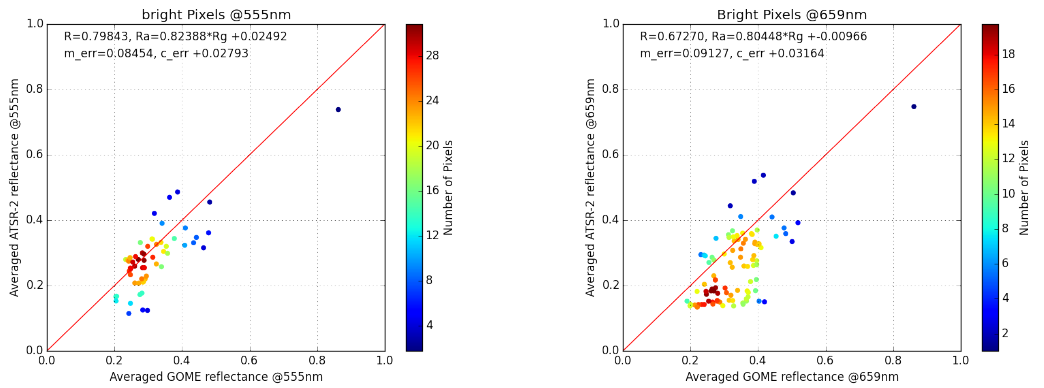

Figure A.3: Scatter plots with linear fit of spectrally averaged GOME reflectance against spatially averaged ATSR-2 reflectance at 555nm and 659nm for different scenarios for January 1997 data.

All pixels

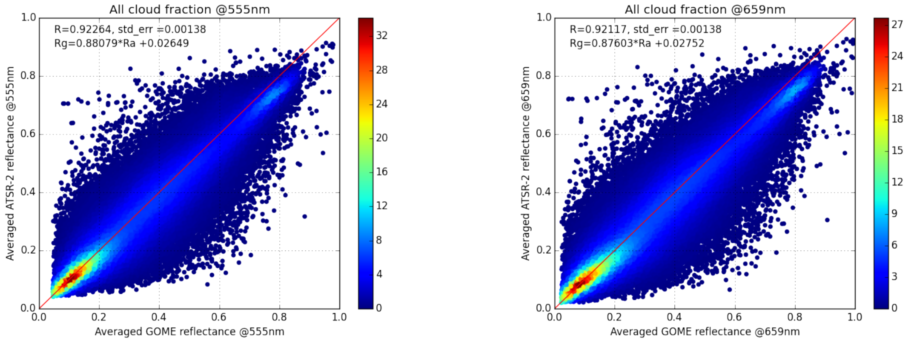

Cloudy pixels

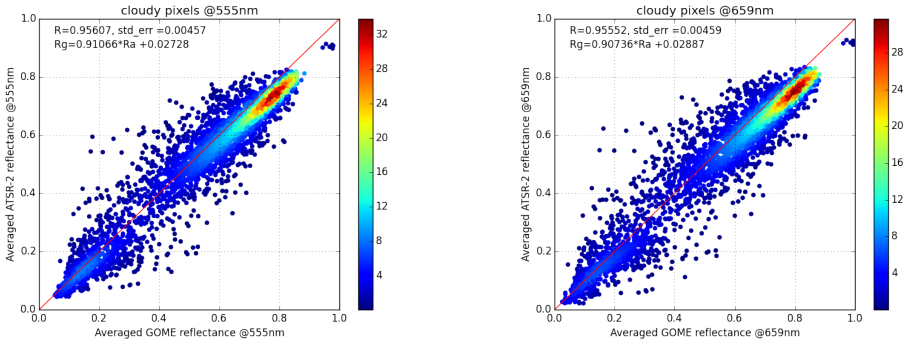

Dark pixels

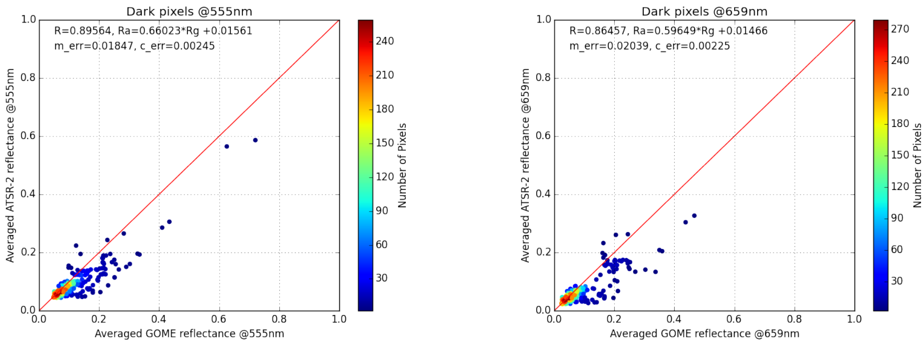

Bright pixels

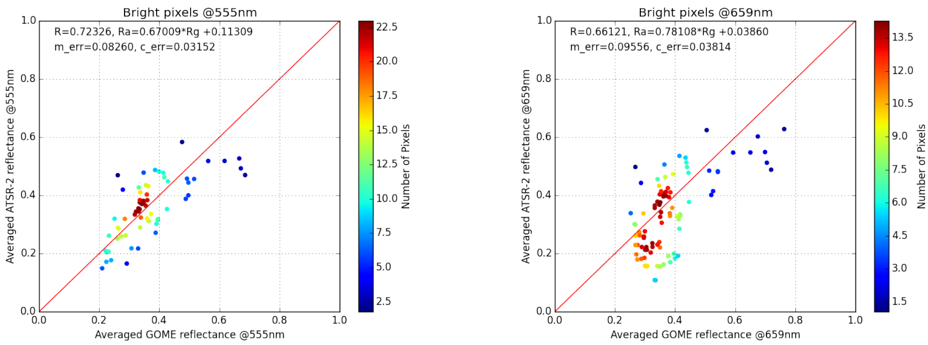

Figure A.4: Scatter plots with linear fit of spectrally averaged GOME reflectance against spatially averaged ATSR-2 reflectance at 555nm and 659nm for different scenarios for February 1997 data.

All pixels

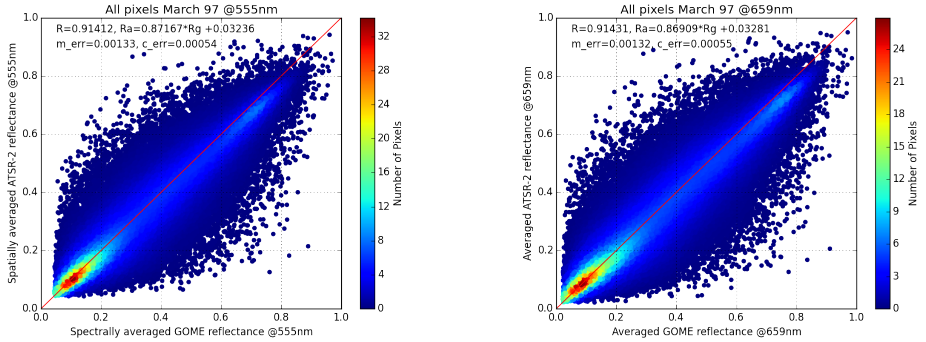

Cloudy pixels

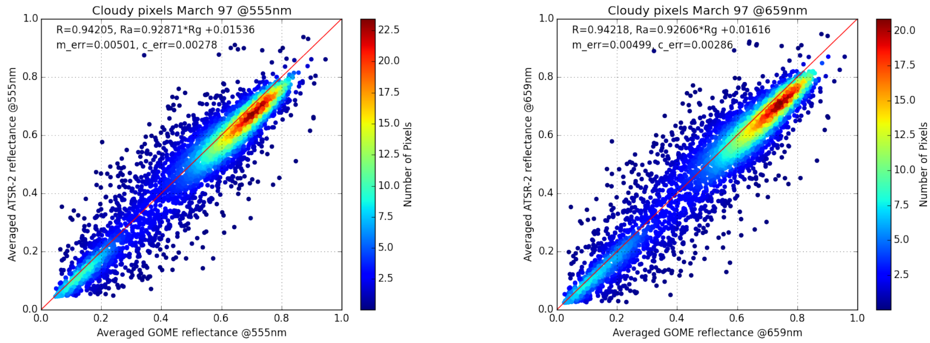

Dark pixels

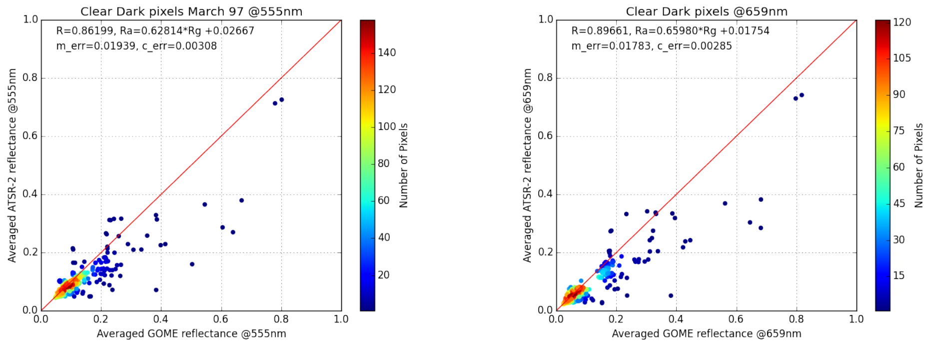

Bright pixels

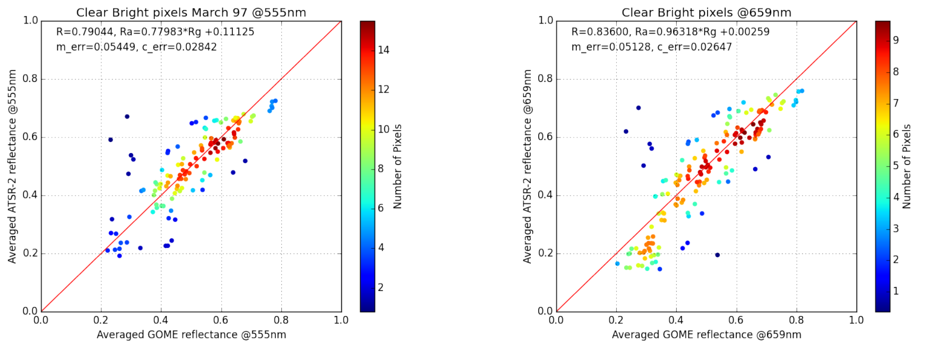

Figure A.5: Scatter plots with linear fit of spectrally averaged GOME reflectance against spatially averaged ATSR-2 reflectance at 555nm and 659nm for different scenarios for March 1997 data.

All pixels

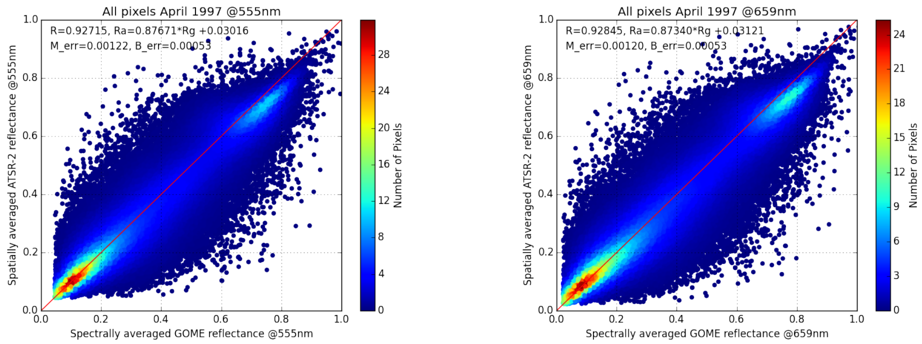

Cloudy pixels

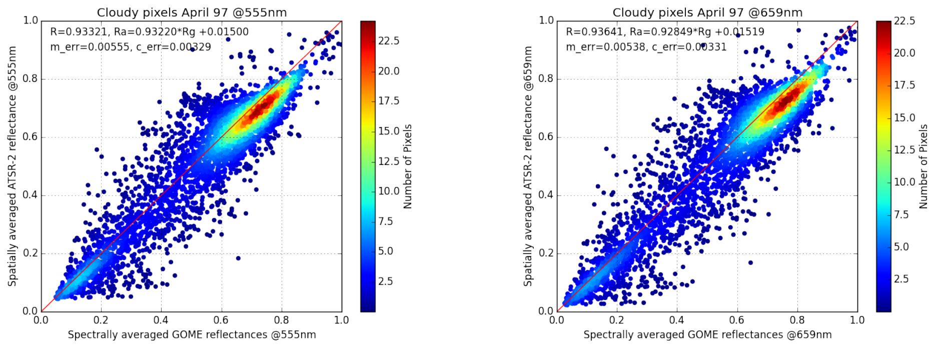

Dark pixels

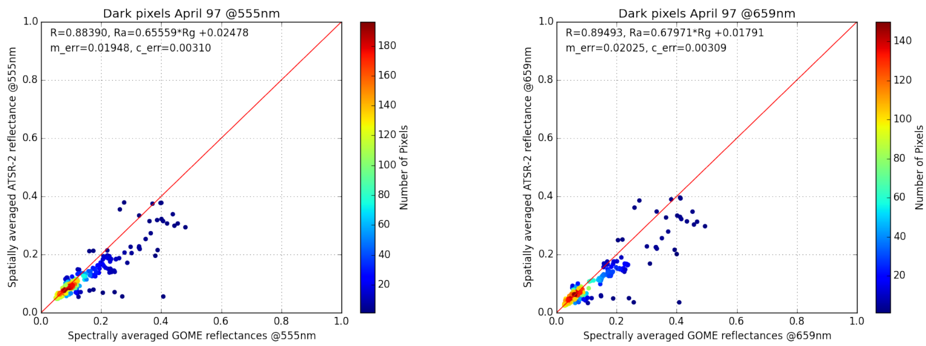

Bright pixels

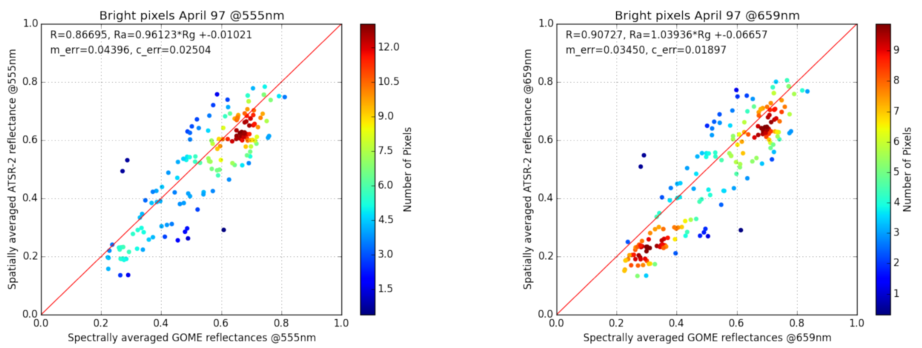

Figure A.6: Scatter plots with linear fit of spectrally averaged GOME reflectance against spatially averaged ATSR-2 reflectance at 555nm and 659nm for different scenarios for April 1997 data.

All pixels

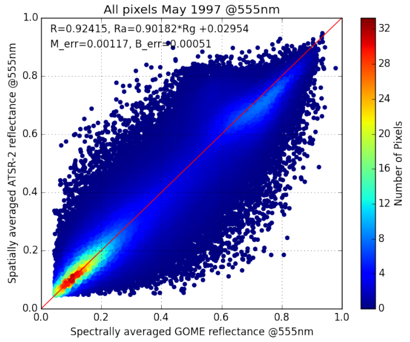

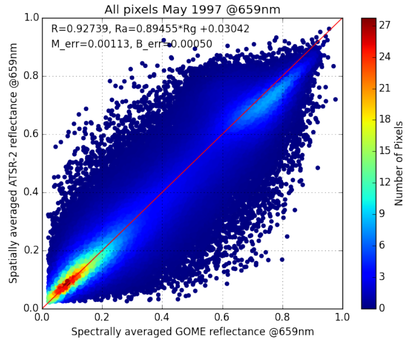

Cloudy pixels

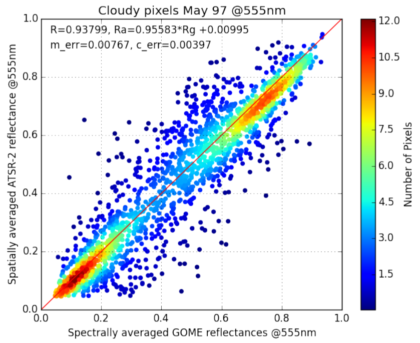

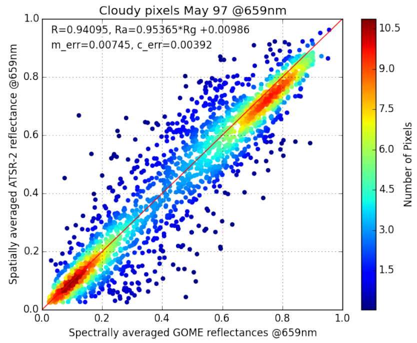

Dark pixels

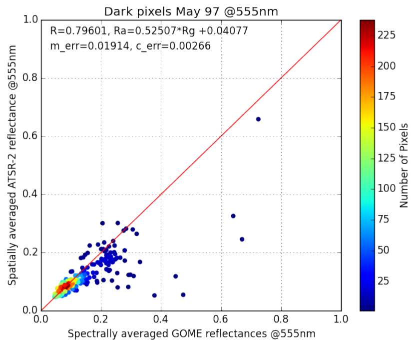

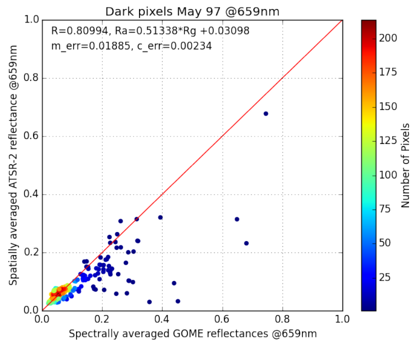

Bright pixels

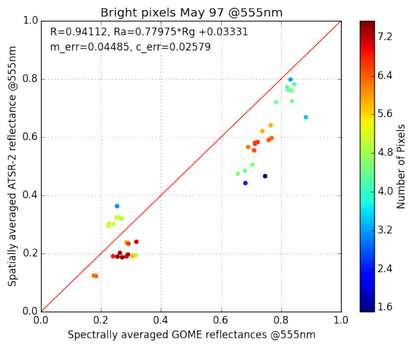

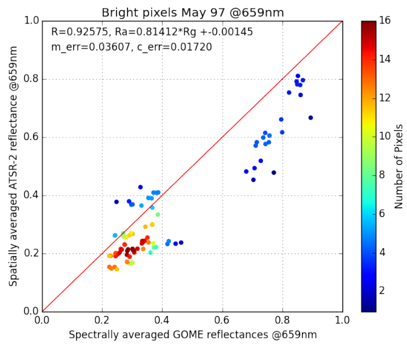

Figure A.7: Scatter plots with linear fit of spectrally averaged GOME reflectance against spatially averaged ATSR-2 reflectance at 555nm and 659nm for different scenarios for May 1997 data.

All pixels

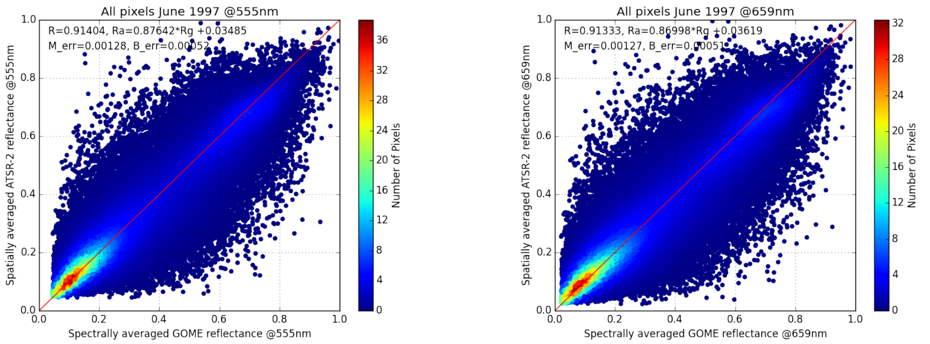

Cloudy pixels

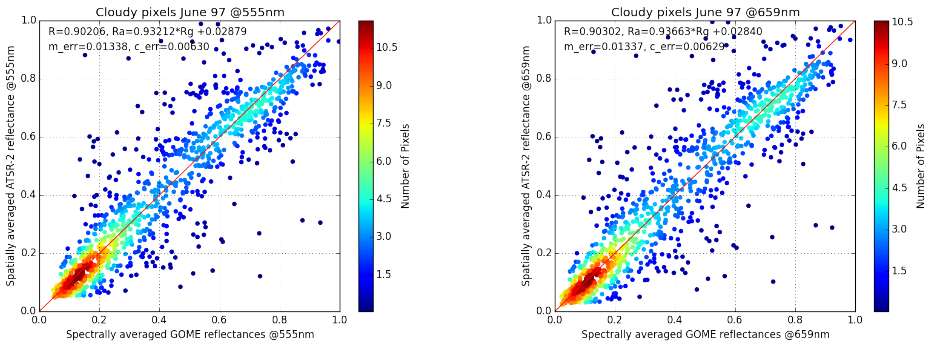

Dark pixels

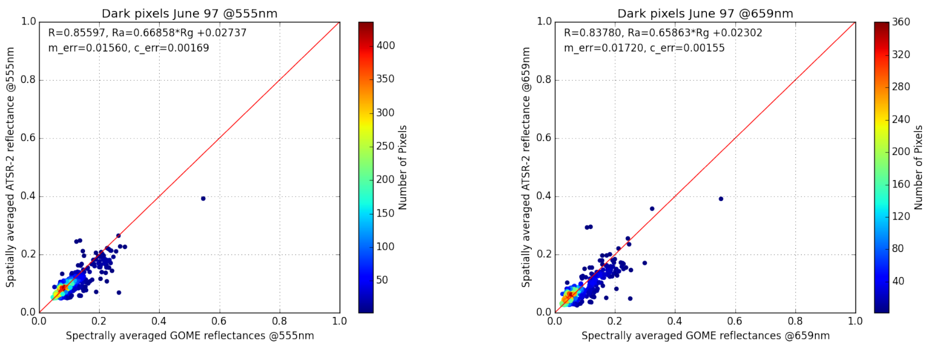

Bright pixels

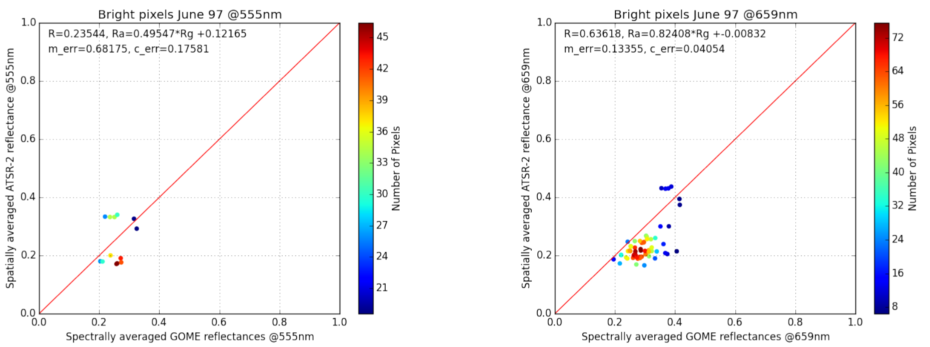

Figure A.8: Scatter plots with linear fit of spectrally averaged GOME reflectance against spatially averaged ATSR-2 reflectance at 555nm and 659nm for different scenarios for June 1997 data.

Cloudy pixels

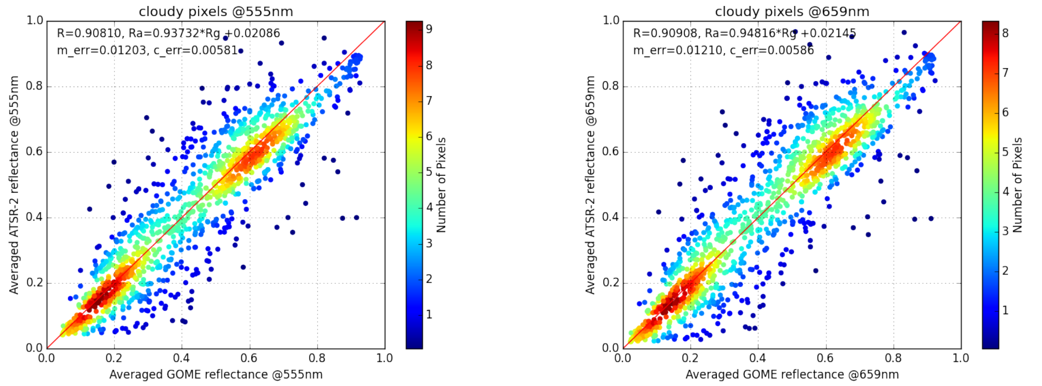

Dark pixels

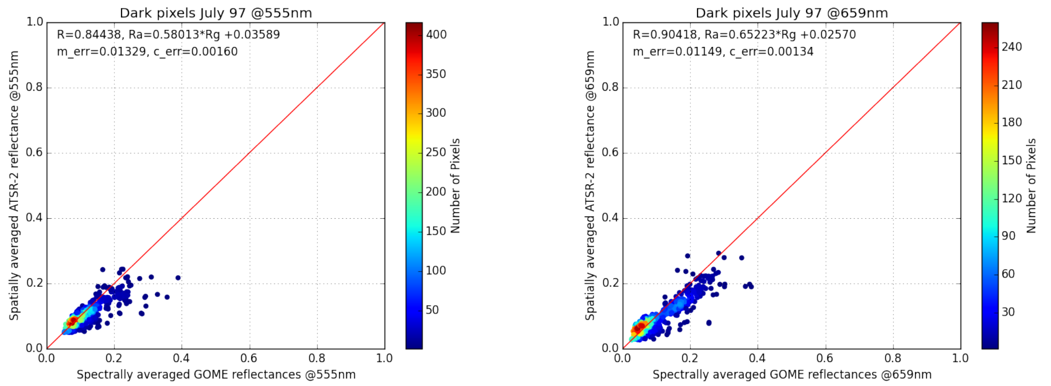

Bright pixels

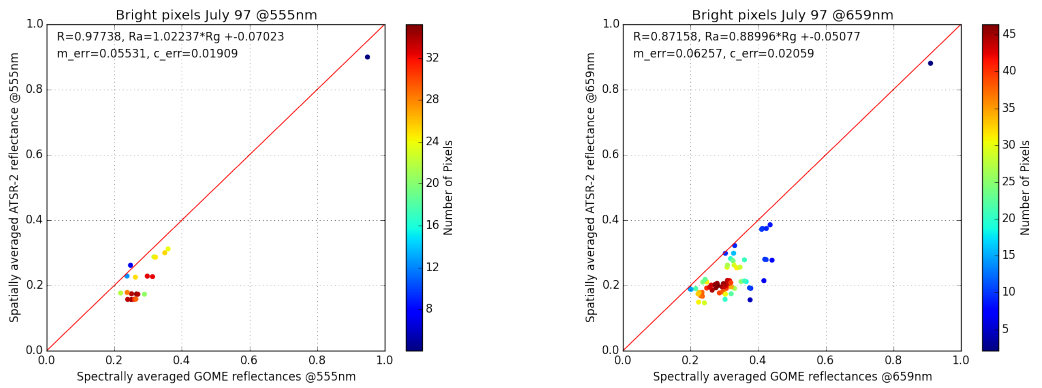

Figure A.9: Scatter plots with linear fit of spectrally averaged GOME reflectance against spatially averaged ATSR-2 reflectance at 555nm and 659nm for different scenarios for July 1997 data.

All pixels

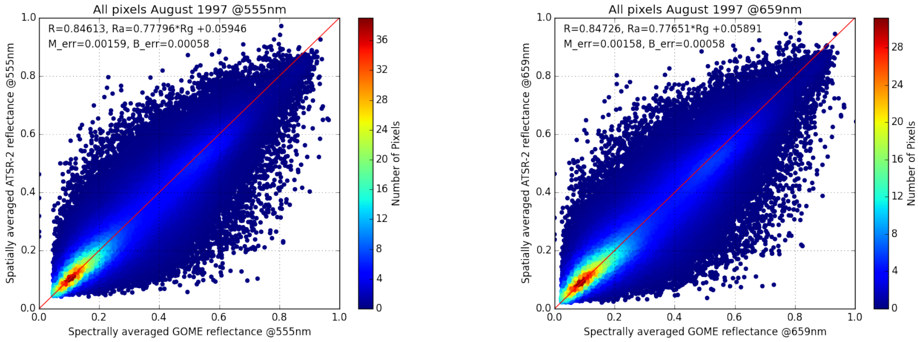

Cloudy pixels

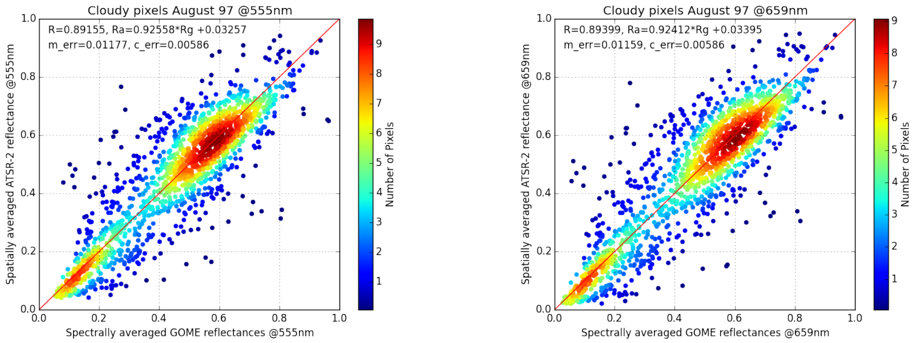

Dark pixels

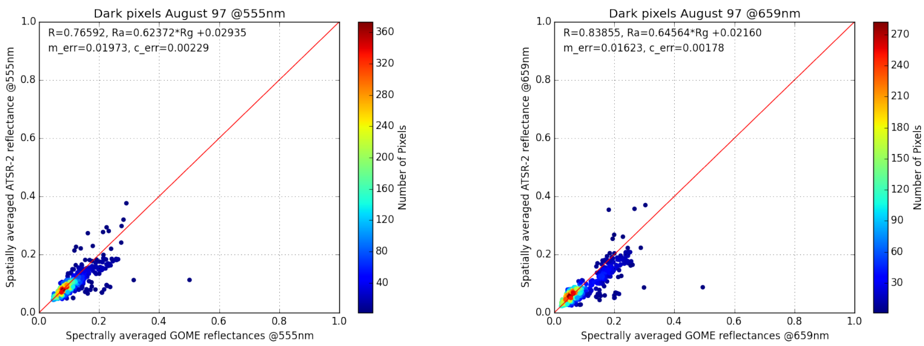

Bright pixels

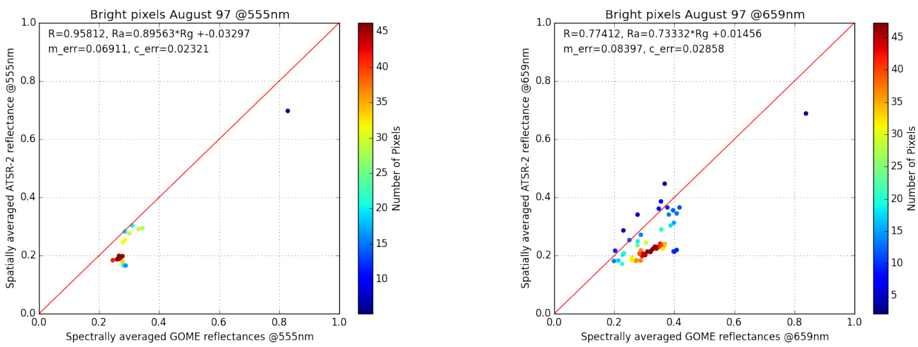

Figure A.10: Scatter plots with linear fit of spectrally averaged GOME reflectance against spatially averaged ATSR-2 reflectance at 555nm and 659nm for different scenarios for August 1997 data.

All pixels

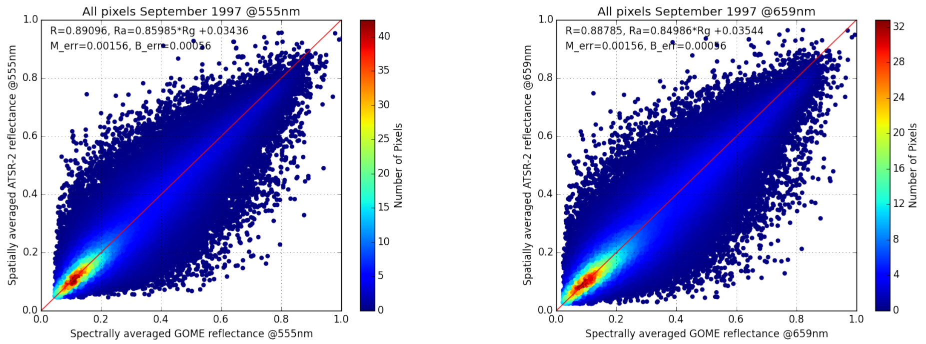

Cloudy pixels

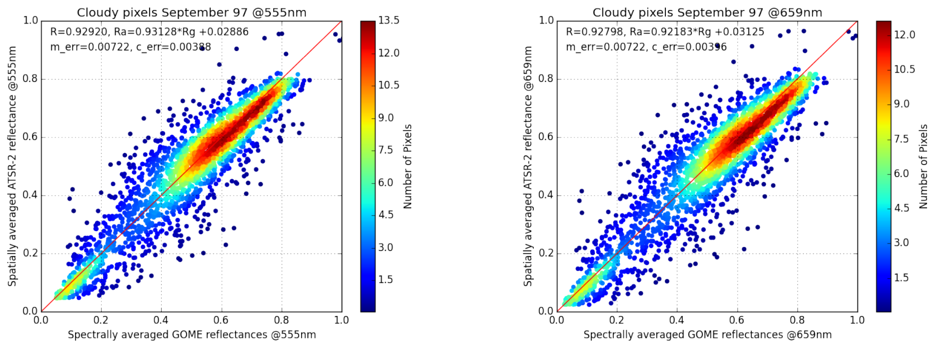

Dark pixels

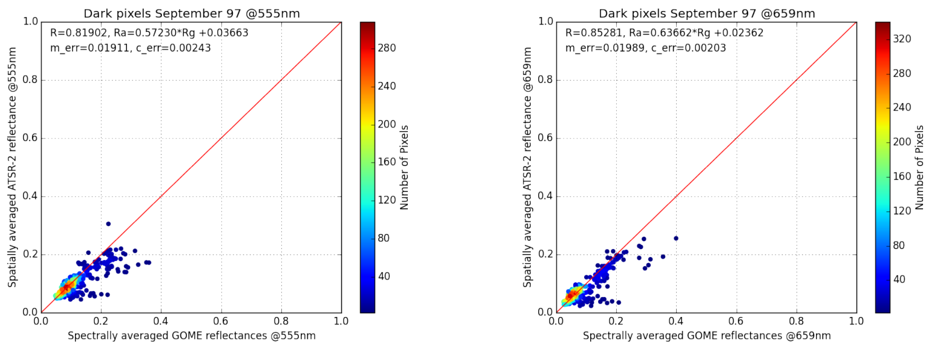

Bright pixels

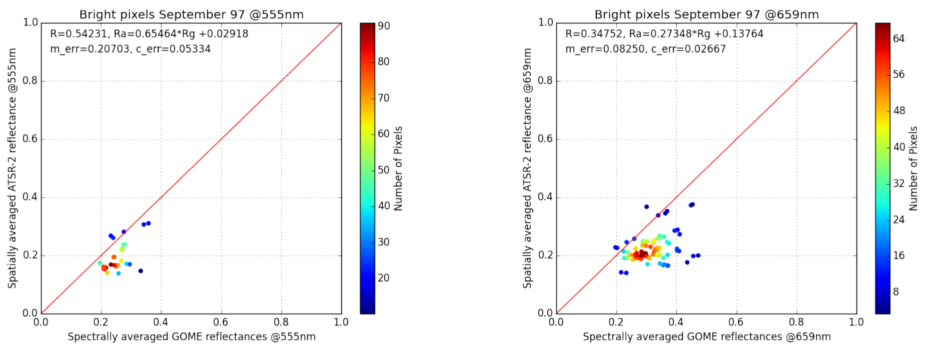

Figure A.11: Scatter plots with linear fit of spectrally averaged GOME reflectance against spatially averaged ATSR-2 reflectance at 555nm and 659nm for different scenarios for September 1997 data.

All pixels

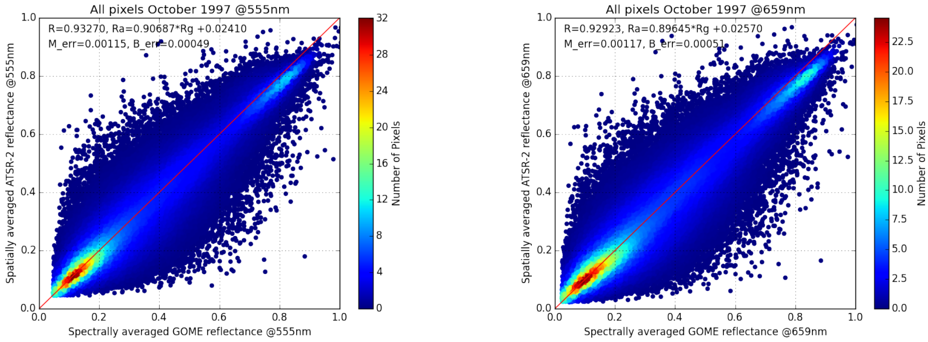

Cloudy pixels

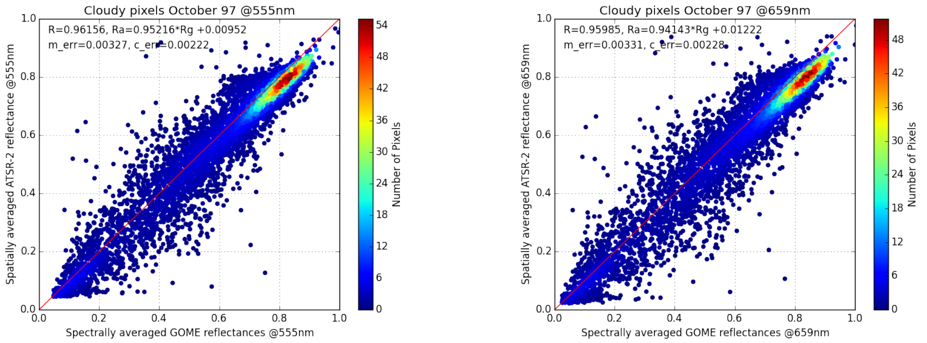

Dark pixels

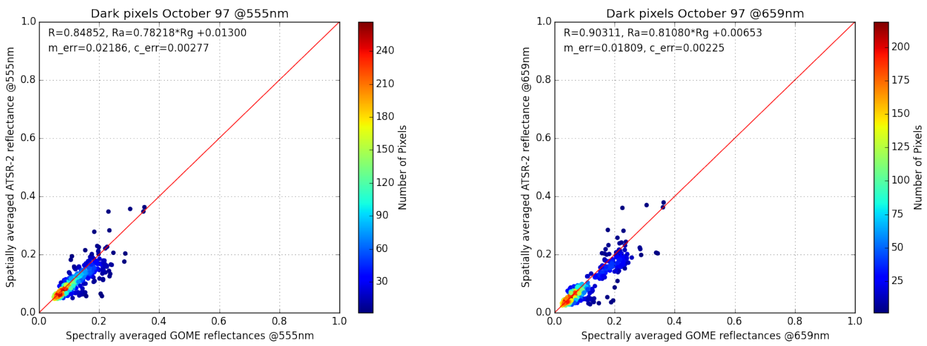

Bright pixels

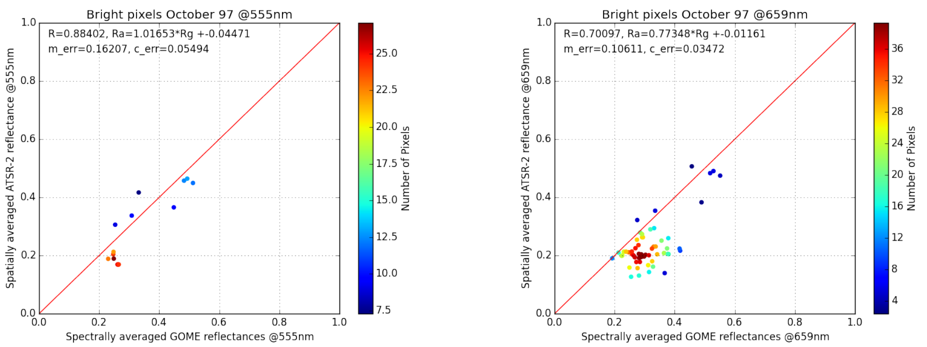

Figure A.12: Scatter plots with linear fit of spectrally averaged GOME reflectance against spatially averaged ATSR-2 reflectance at 555nm and 659nm for different scenarios for October 1997 data.

All pixels

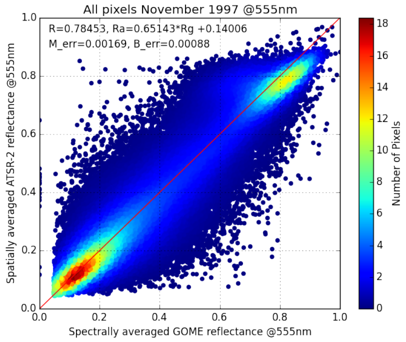

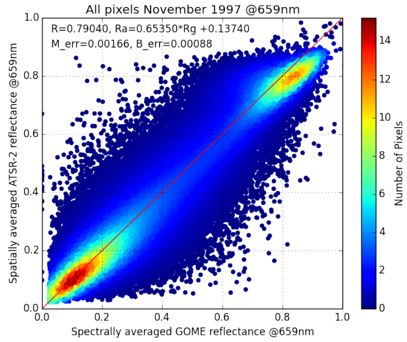

Cloudy pixels

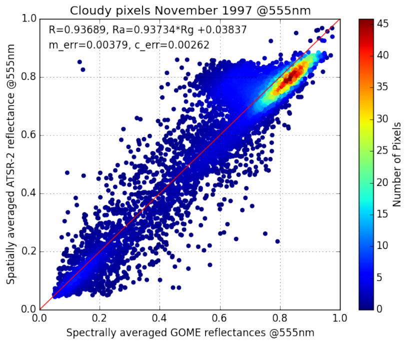

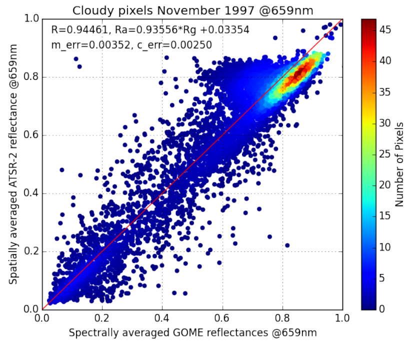

Dark pixels

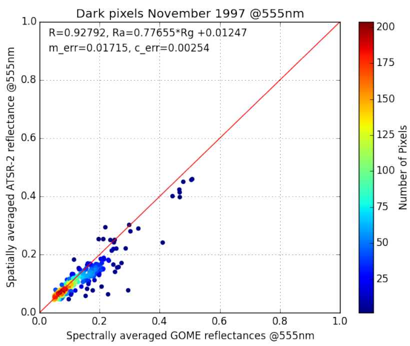

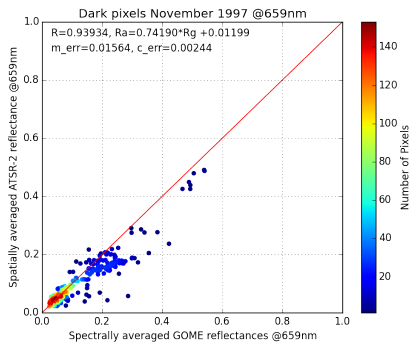

Bright pixels

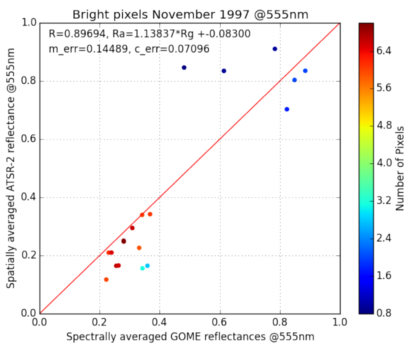

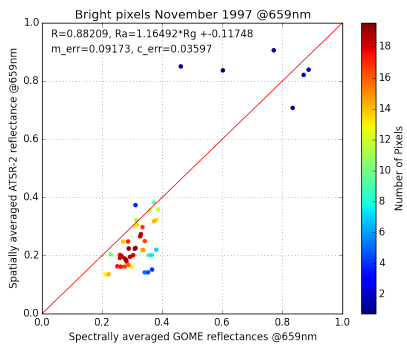

Figure A.13: Scatter plots with linear fit of spectrally averaged GOME reflectance against spatially averaged ATSR-2 reflectance at 555nm and 659nm for different scenarios for November 1997 data.

All pixels

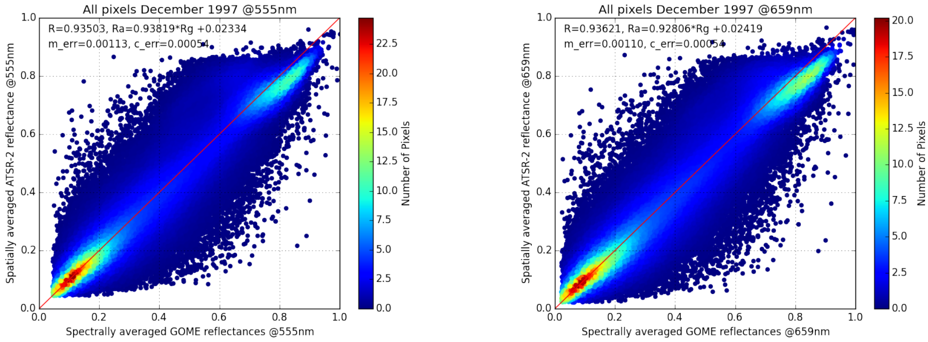

Cloudy pixels

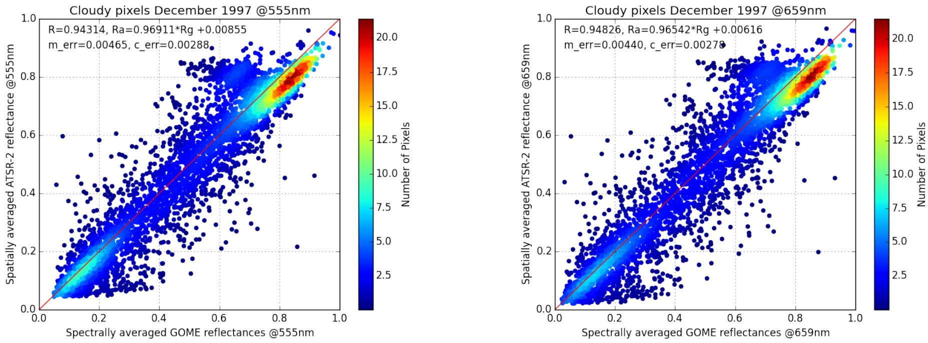

Dark pixels

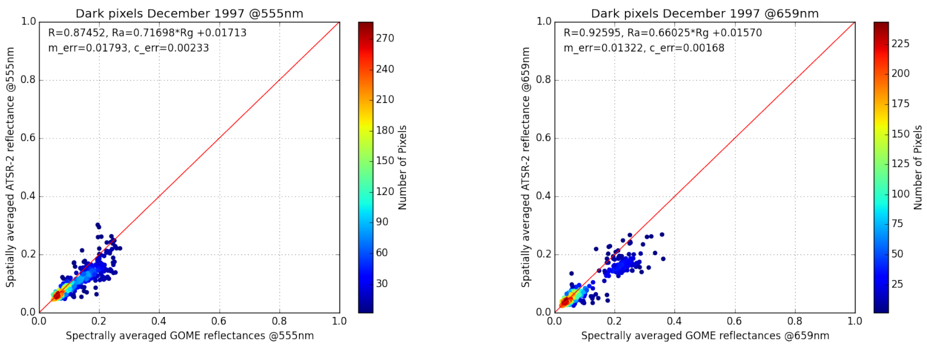

Bright pixels

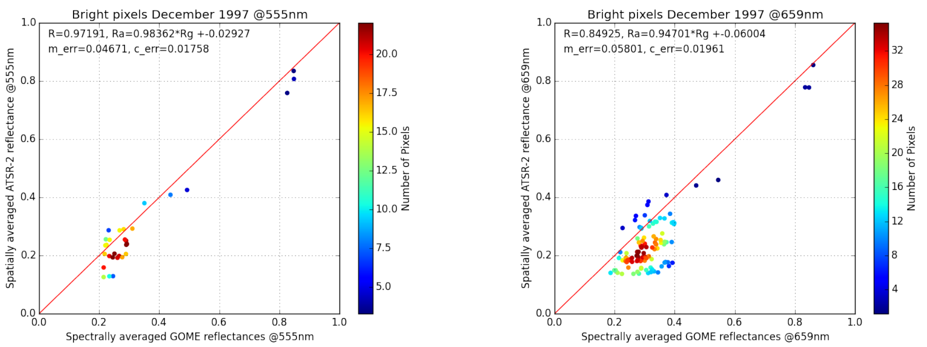

Figure A.14: Scatter plots with linear fit of spectrally averaged GOME reflectance against spatially averaged ATSR-2 reflectance at 555nm and 659nm for different scenarios for December 1997 data.

All pixels

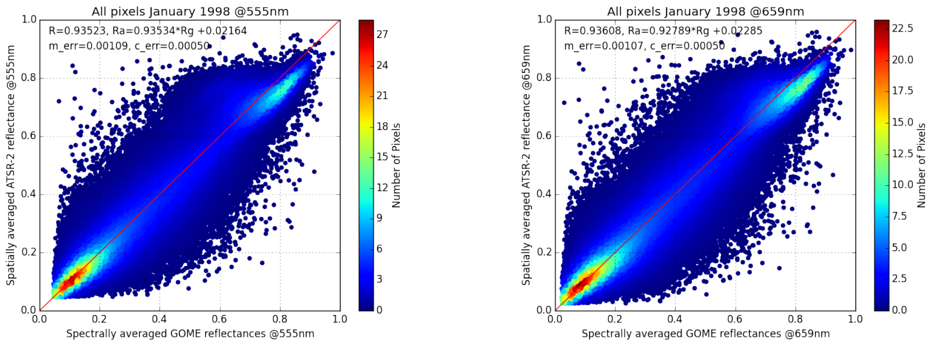

Cloudy pixels

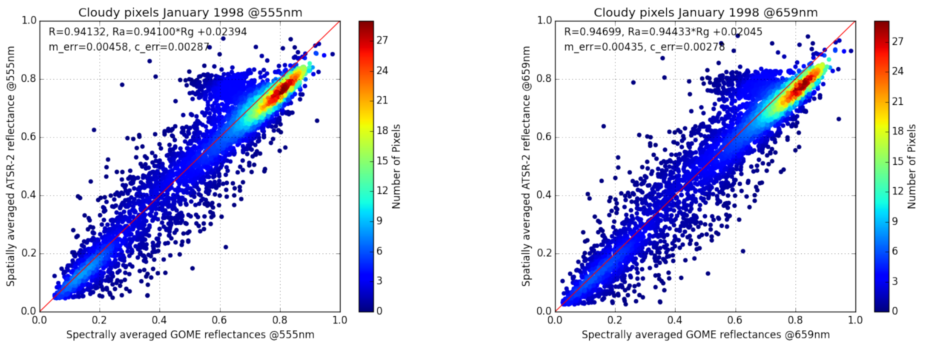

Dark pixels

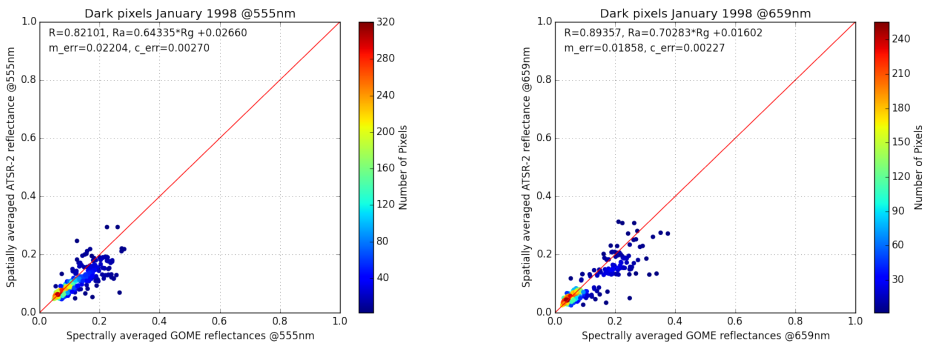

Bright pixels

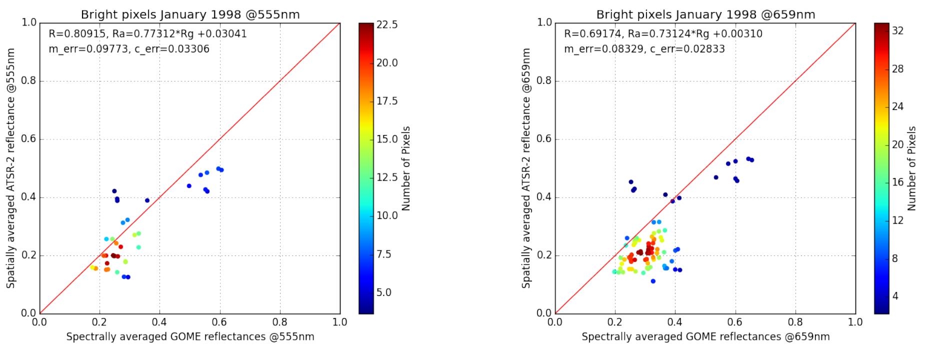

Figure A.15: Scatter plots with linear fit of spectrally averaged GOME reflectance against spatially averaged ATSR-2 reflectance at 555nm and 659nm for different scenarios for January 1998 data.

All pixels

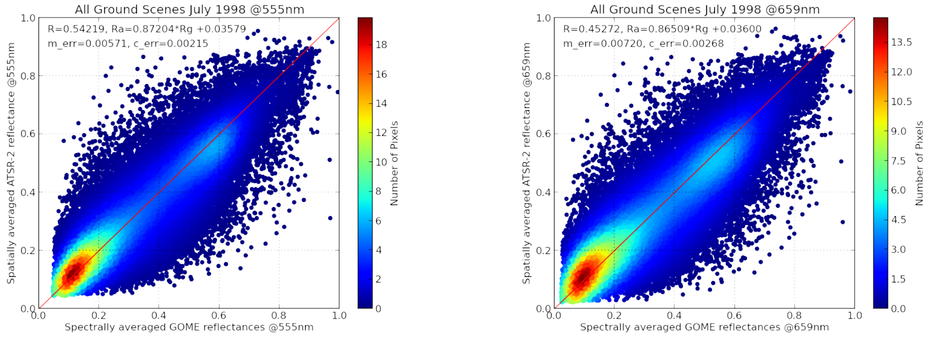

Cloudy pixels

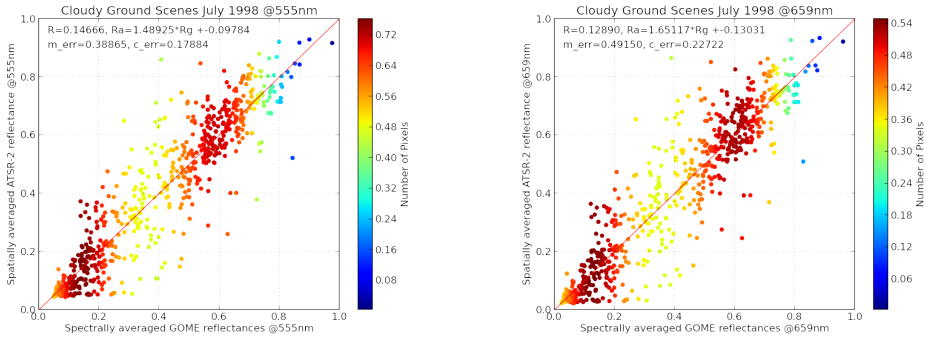

Dark pixels

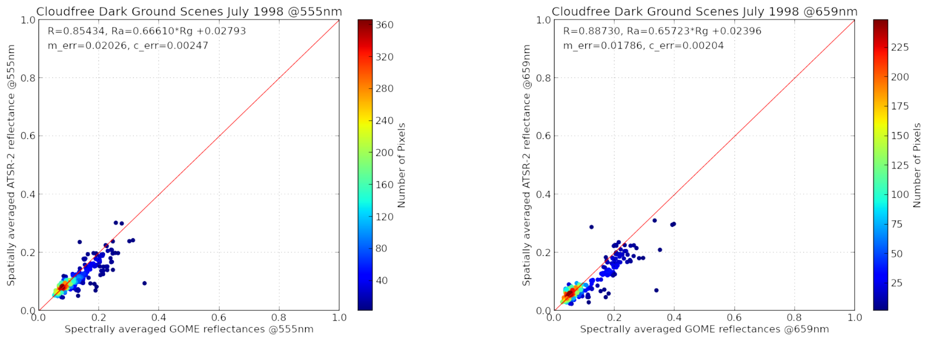

Bright pixels

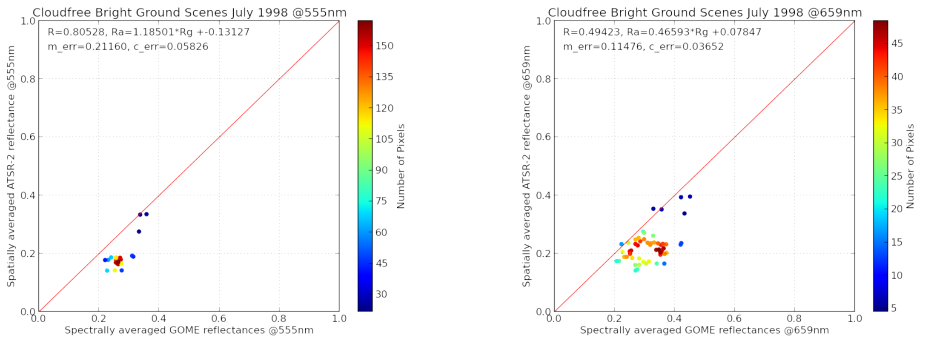

Figure A.16: Scatter plots with linear fit of spectrally averaged GOME reflectance against spatially averaged ATSR-2 reflectance at 555nm and 659nm for different scenarios for July 1998 data.

All pixels

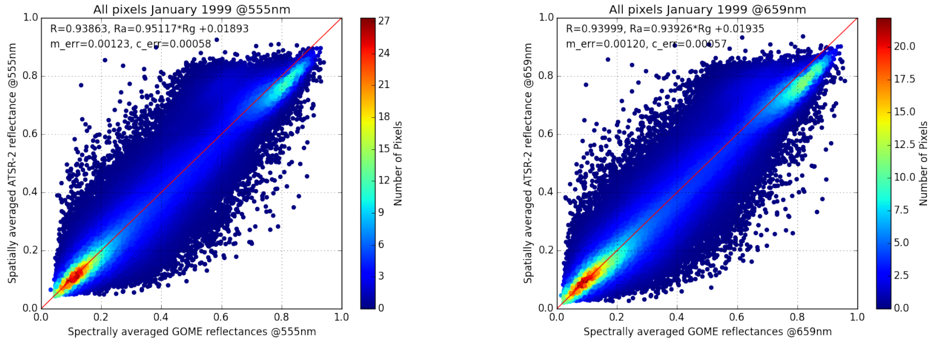

Cloudy pixels

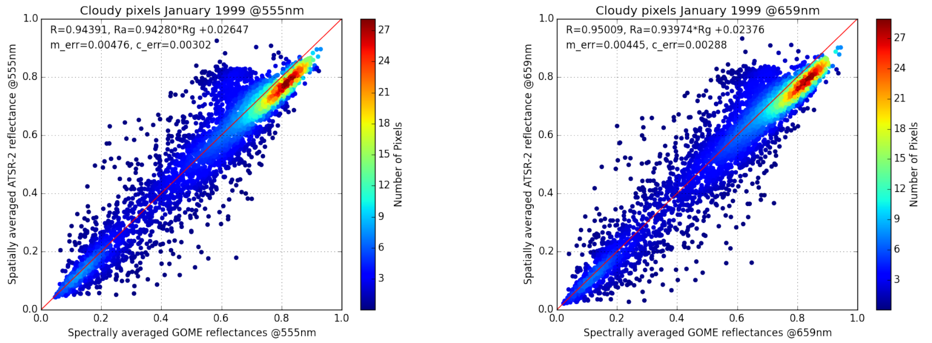

Dark pixels

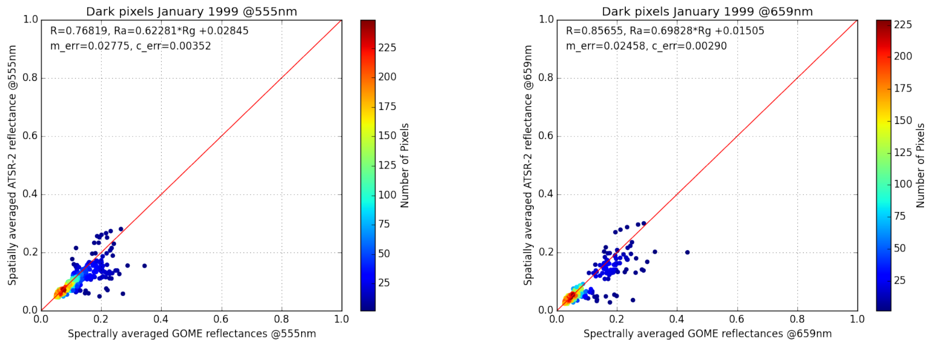

Bright pixels

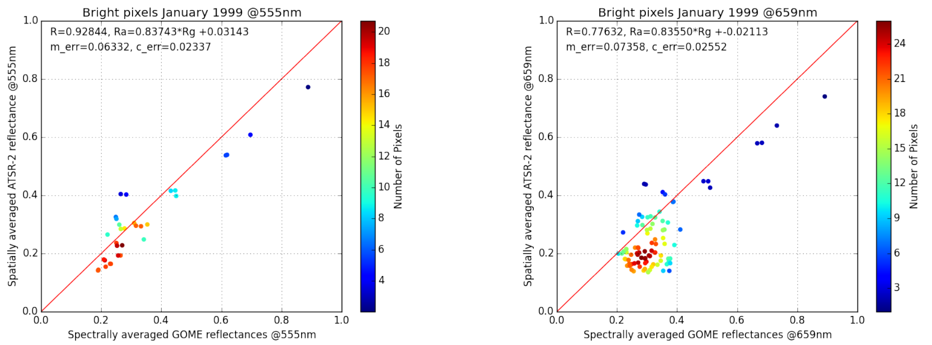

Figure A.17: Scatter plots with linear fit of spectrally averaged GOME reflectance against spatially averaged ATSR-2 reflectance at 555nm and 659nm for different scenarios for January 1999 data.

All pixels

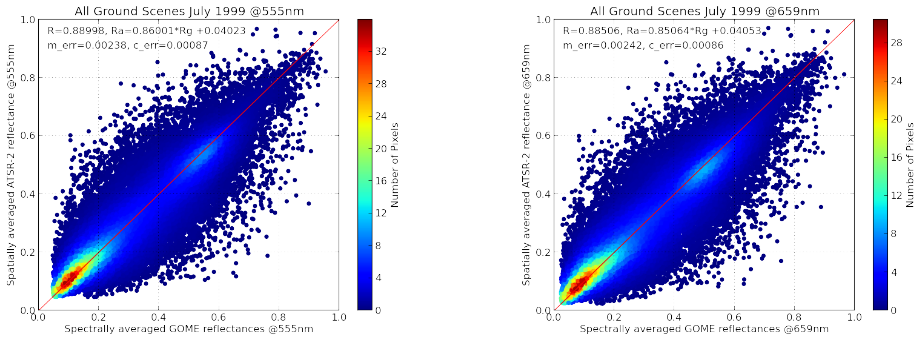

Cloudy pixels

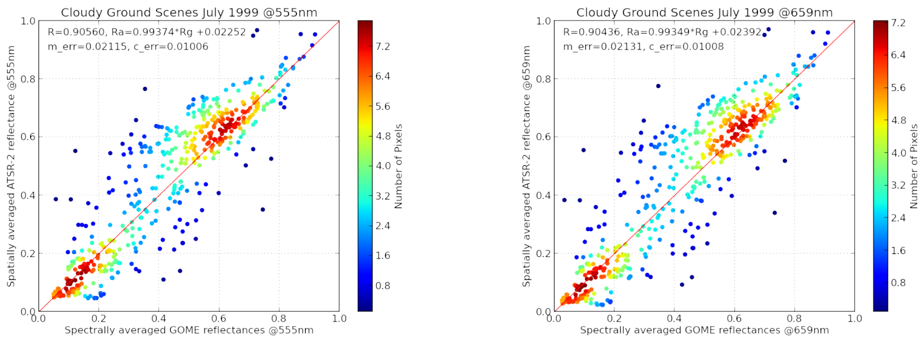

Dark pixels

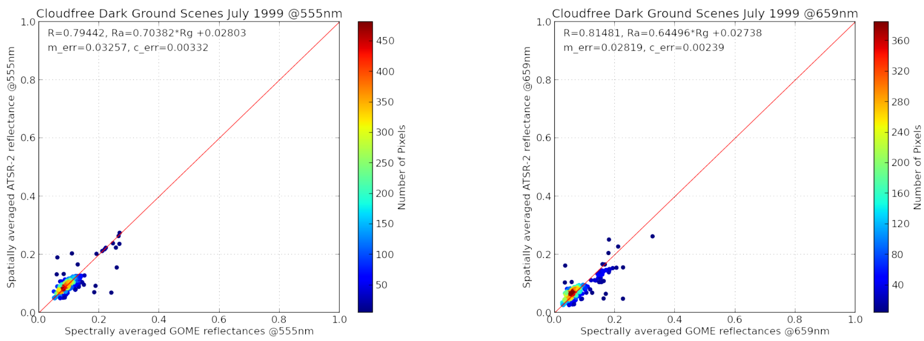

Bright pixels

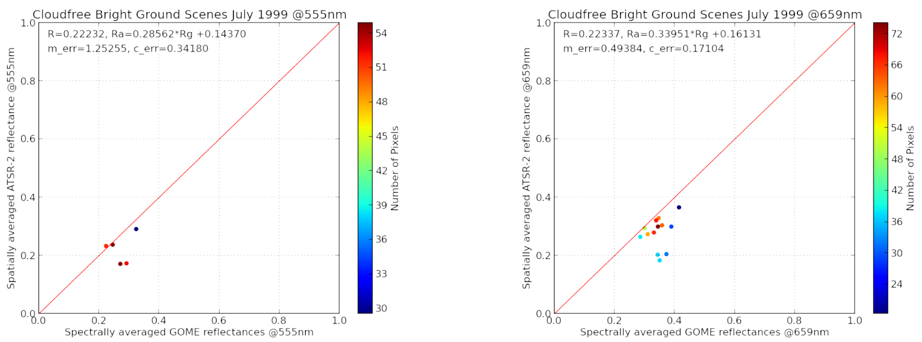

Figure A.18: Scatter plots with linear fit of spectrally averaged GOME reflectance against spatially averaged ATSR-2 reflectance at 555nm and 659nm for different scenarios for July 1999 data.

All pixels

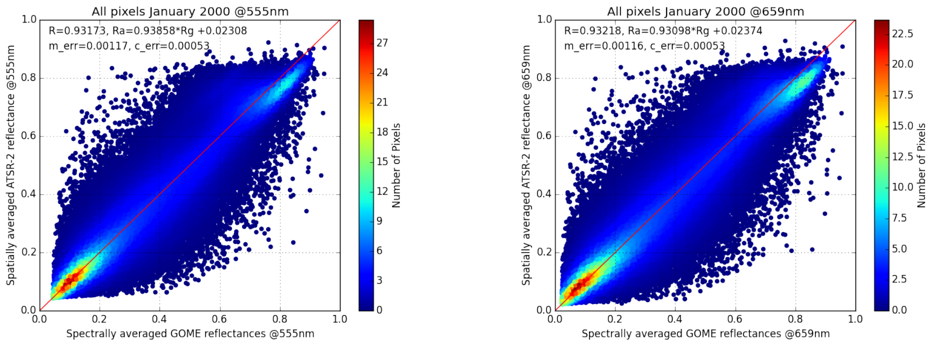

Cloudy pixels

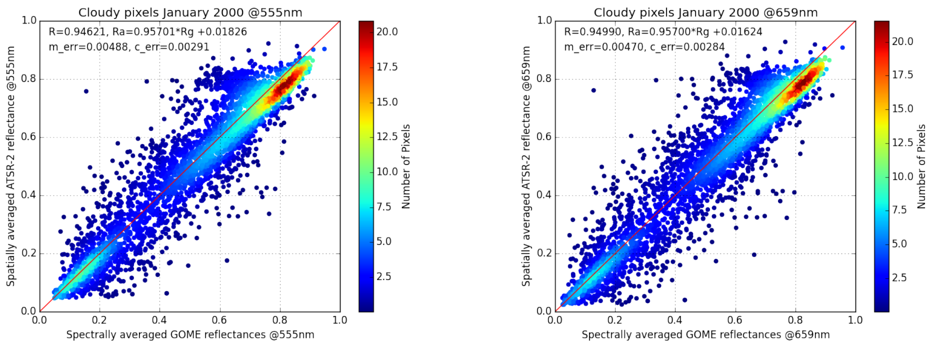

Dark pixels

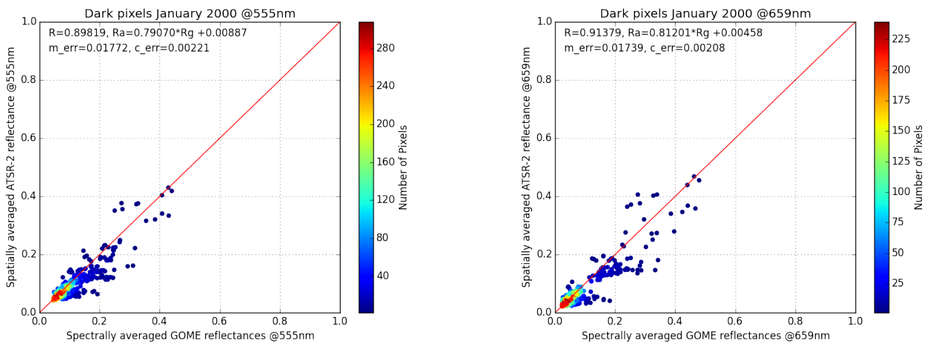

Bright pixels

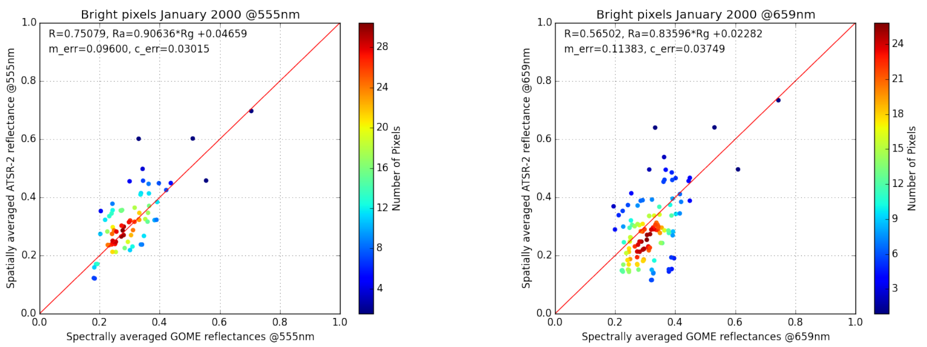

Figure A.19: Scatter plots with linear fit of spectrally averaged GOME reflectance against spatially averaged ATSR-2 reflectance at 555nm and 659nm for different scenarios for January 2000 data.

All pixels

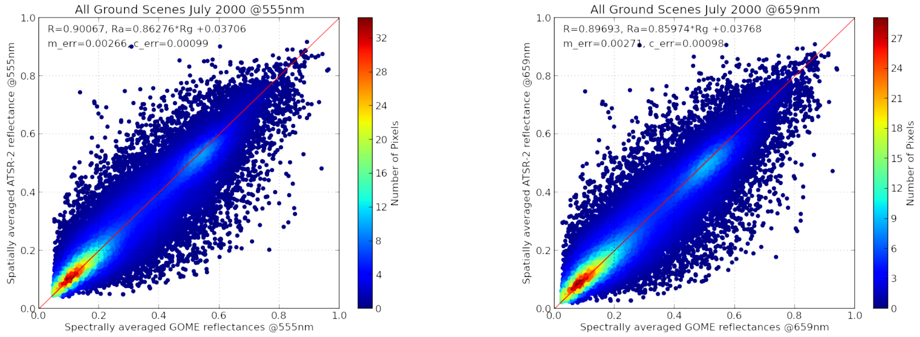

Cloudy pixels

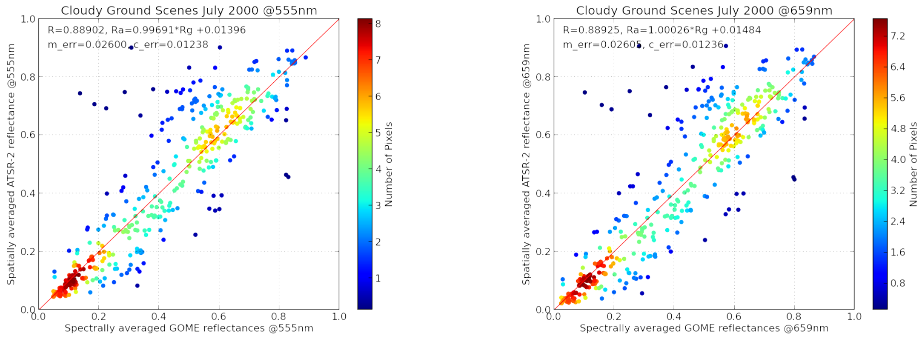

Dark pixels

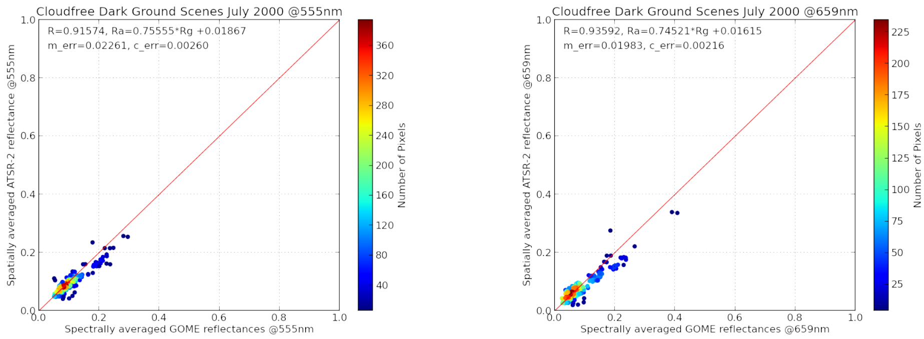

Bright pixels

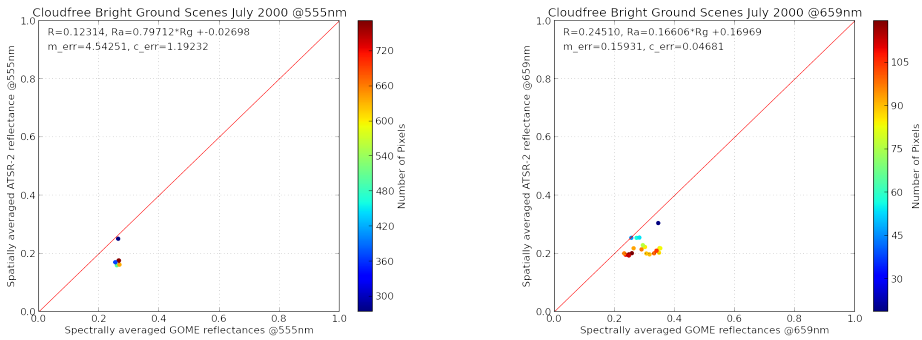

Figure A.20: Scatter plots with linear fit of spectrally averaged GOME reflectance against spatially averaged ATSR-2 reflectance at 555nm and 659nm for different scenarios for July 2000 data.

All pixels

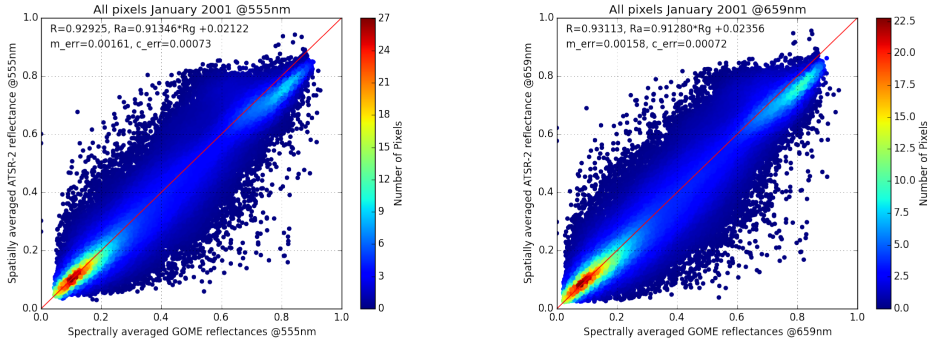

Cloudy pixels

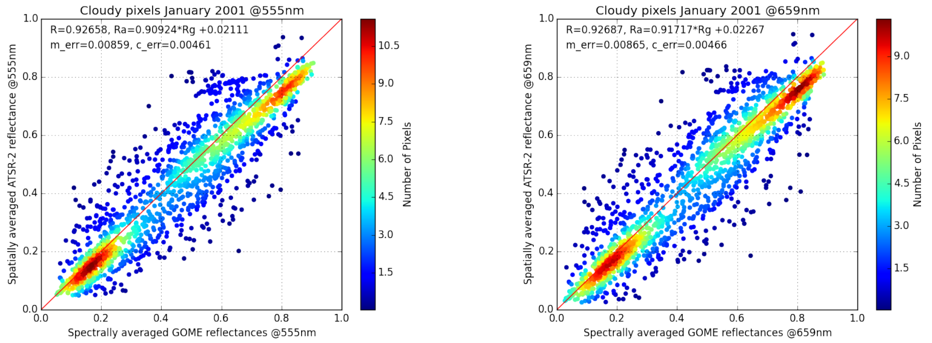

Dark pixels

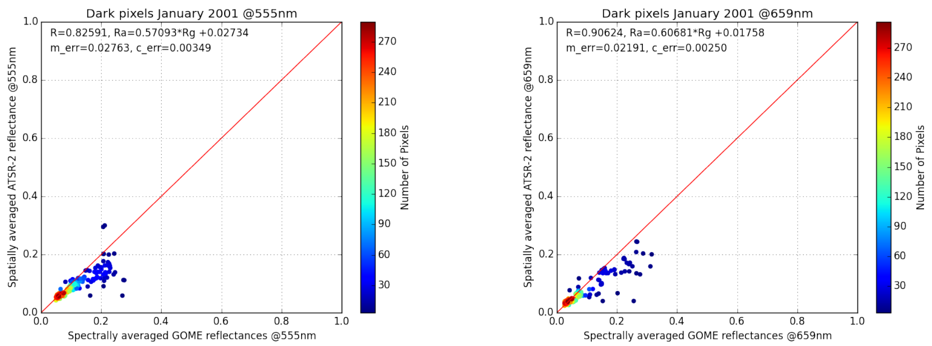

Bright pixels

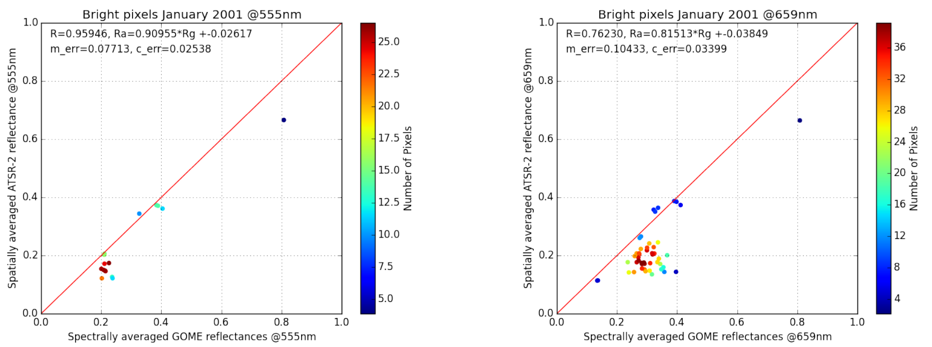

Figure A.21: Scatter plots with linear fit of spectrally averaged GOME reflectance against spatially averaged ATSR-2 reflectance at 555nm and 659nm for different scenarios for January 2001 data.

All pixels

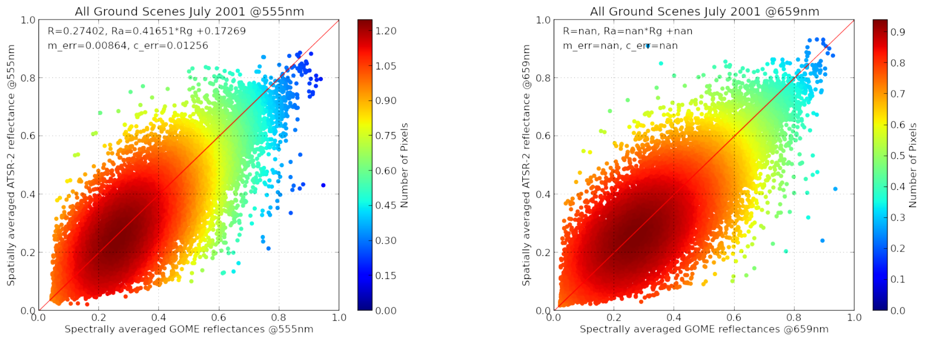

Cloudy pixels

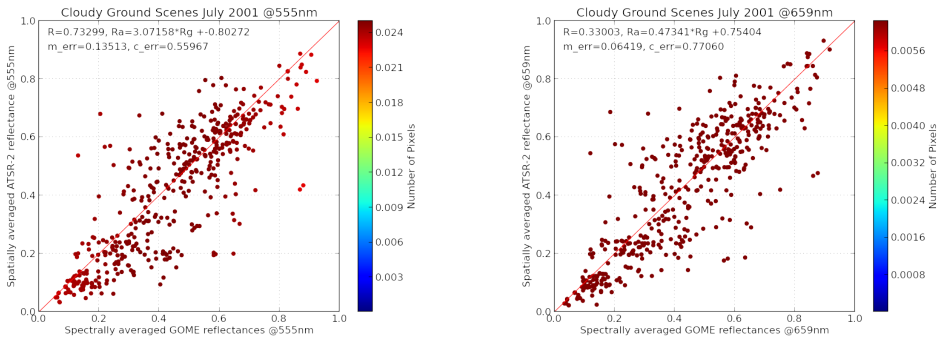

Dark pixels

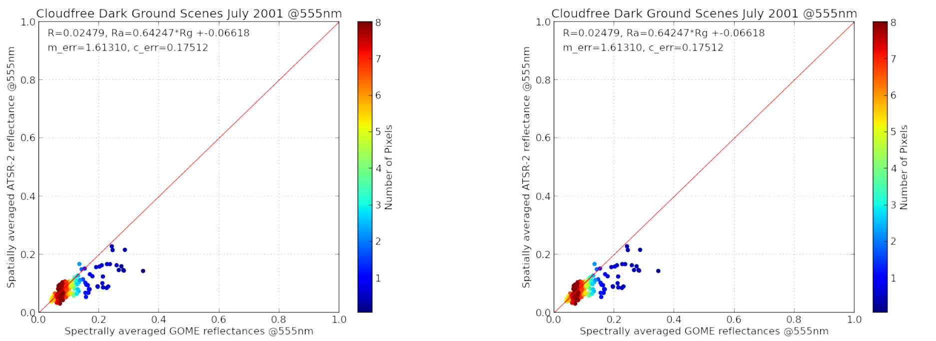

Bright pixels

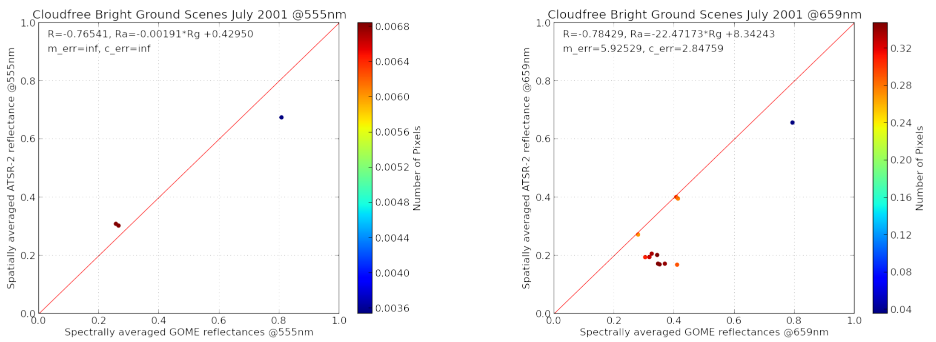

Figure A.22: Scatter plots with linear fit of spectrally averaged GOME reflectance against spatially averaged ATSR-2 reflectance at 555nm and 659nm for different scenarios for July 2001 data.

All pixels

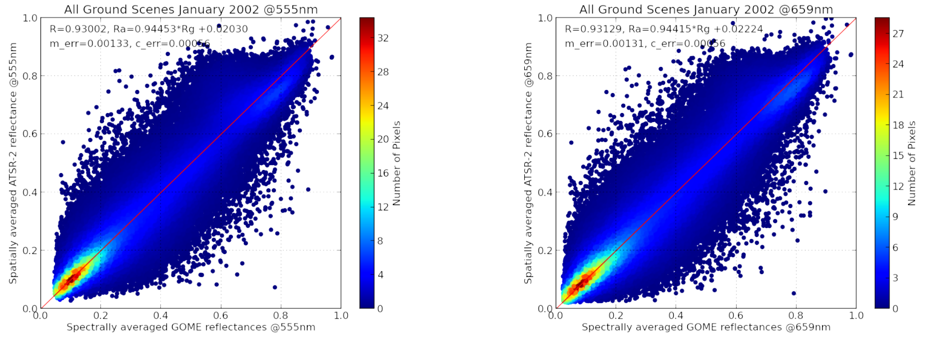

Cloudy pixels

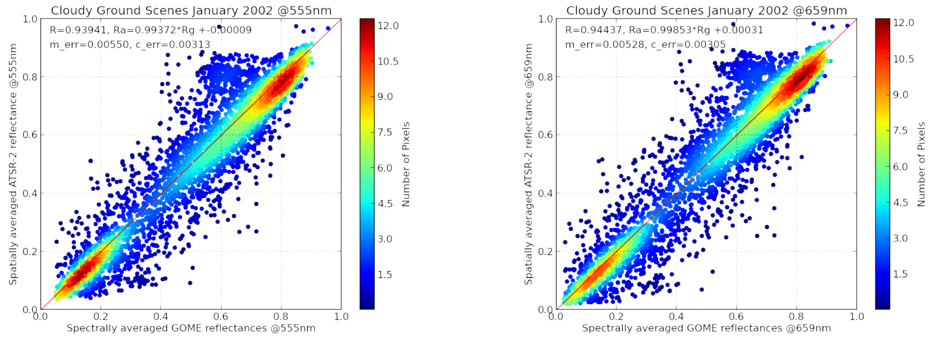

Dark pixels

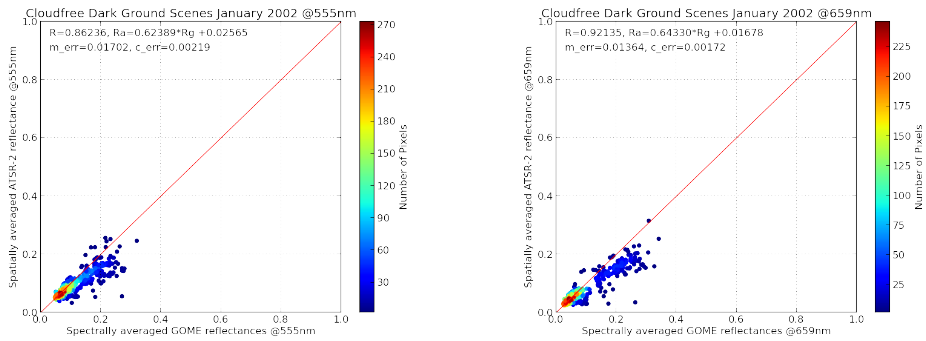

Bright pixels

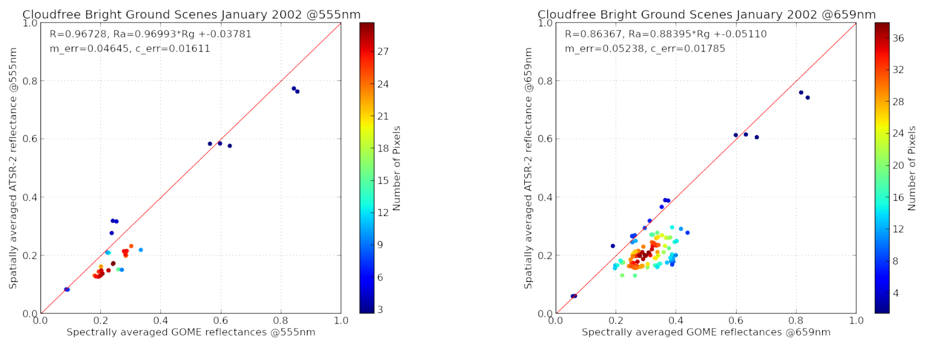

Figure A.23: Scatter plots with linear fit of spectrally averaged GOME reflectance against spatially averaged ATSR-2 reflectance at 555nm and 659nm for different scenarios for January 2002 data.

All pixels

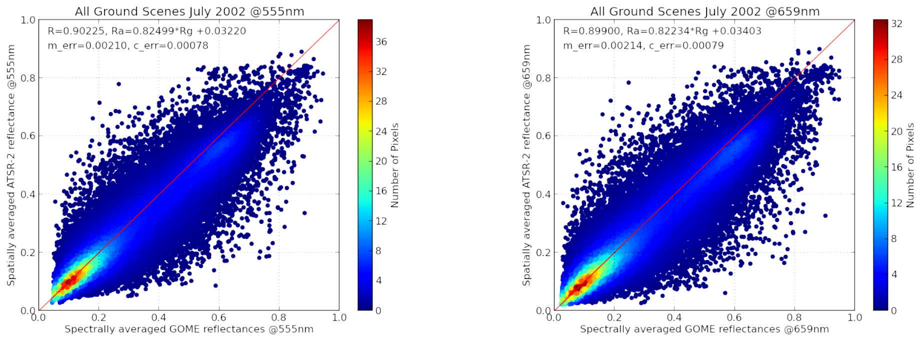

Cloudy pixels

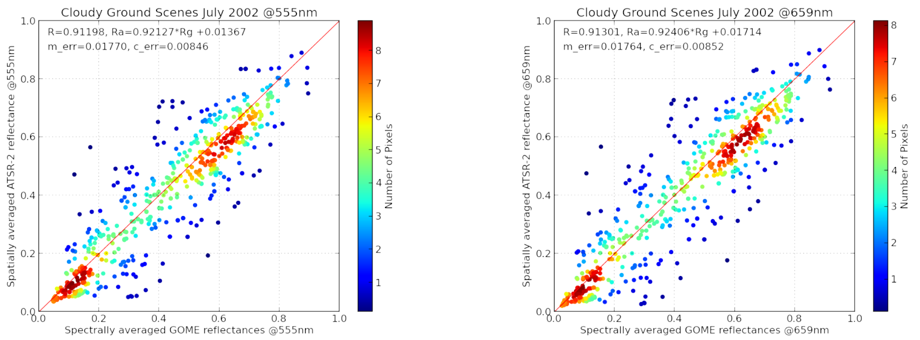

Dark pixels

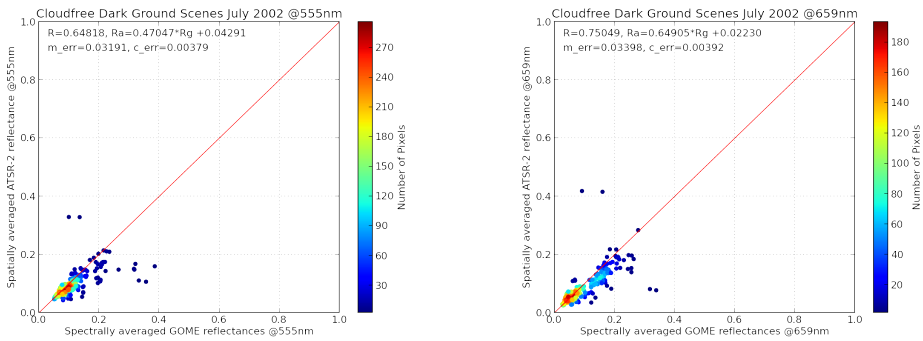

Bright pixels

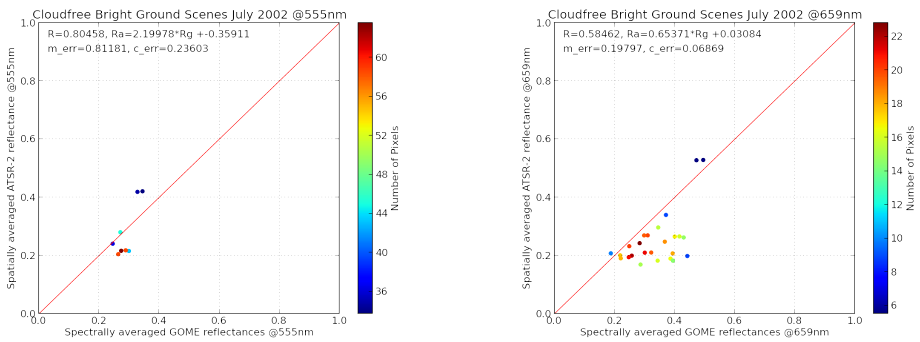

Figure A.24: Scatter plots with linear fit of spectrally averaged GOME reflectance against spatially averaged ATSR-2 reflectance at 555nm and 659nm for different scenarios for July 2002 data.

List of Figures

List of Tables

Acknowledgment

Foremost, my sincere thanks goes to my supervisor Dr. Mark Weber for offering me the opportunity to do my thesis with his group (UV-SAT) and also his systematic guidance through out the duration of my work.

I would like to express my sincere gratitude to my advisor Stefan Boetel for the continuous support, for his patience, motivation and immense knowledge. His guidance helped me in all time of research and writing of this thesis.

I would also like to thank the rest of my office colleague: Dr Thoma Krings and Martin Budde, for their encouragement, insightful comments.
I am indebted to Mr and Mrs. Obinna A. Ezejiofor, for their moral support during difficult times.
Finally, i take this opportunity to express the profound gratitude from my heart to my beloved parents, and my siblings for their love, support and endless prayers.